

1 Rigorous Observational Tests Contradict the Accelerating Moment Release Hypothesis

2

3 Jeanne L. Hardebeck¹, Karen R. Felzer², and Andrew J. Michael¹

4

5 ¹ USGS MS 977, 345 Middlefield Road, Menlo Park, CA 94025, jhardebeck@usgs.gov,

6 michael@usgs.gov

7 ² USGS, 525 South Wilson Av., Pasadena, CA 91106, kfelzer@gps.caltech.edu

8

9 September 21, 2007 – REVISED 2/4/2008

10

11

11 1. Abstract

12 We test the hypothesis that accelerating moment release (AMR) is a precursor to large
13 earthquakes, using data from California, Nevada, and Sumatra. Spurious cases of AMR
14 can arise from data-fitting because the time period, area, and sometimes magnitude range
15 analyzed before each mainshock are often optimized to produce the strongest AMR
16 signal. Optimizing the search criteria can identify apparent AMR even if no robust signal
17 exists. For both 1950-2006 California-Nevada $M \geq 6.5$ earthquakes and the 2004 $M 9.3$
18 Sumatra earthquake we can find two contradictory patterns in the pre-mainshock
19 earthquakes by data-fitting: AMR and decelerating moment release. We compare the
20 apparent AMR found in the real data to the apparent AMR found in four types of
21 synthetic catalogs with no inherent AMR. When realistic spatiotemporal clustering is
22 included in the simulations, similar AMR signals are found by data-fitting in both the real
23 and synthetic data sets even though the synthetic data sets contain no real AMR. These
24 tests demonstrate that apparent AMR arises from a combination of data-fitting and
25 normal foreshock and aftershock activity. Therefore, AMR has no more predictive power
26 than existing forecasts that more directly and optimally utilize earthquake clustering. In
27 principle, data-fitting artifacts could be avoided if the free parameters were determined
28 from scaling relationships between the duration and spatial extent of the AMR pattern
29 and the magnitude of the earthquake that follows it. However, we demonstrate that
30 previously proposed scaling relationships are unstable, statistical artifacts caused by the
31 use of a minimum magnitude for the earthquake catalog that scales with the mainshock
32 magnitude. Some recent AMR studies have used spatial regions based on hypothetical
33 stress loading patterns, rather than circles, to select the data. We show that previous tests

34 were biased and that unbiased tests do not find this change to the method to be an
35 improvement. The use of declustered catalogs has also been proposed to eliminate the
36 effect of clustering but we demonstrate that this does not increase the statistical
37 significance of AMR. Given the ease with which data-fitting can find desired patterns in
38 seismicity, future studies of AMR-like observations must include complete tests against
39 synthetic catalogs that include realistic spatiotemporal clustering.

40

41

41 2. Introduction

42

43 This study examines whether or not Accelerating Moment Release [e.g. Bowman
44 *et al.*, 1998; and see references in Mignan *et al.*, 2006a] is a statistically significant
45 precursor to large earthquakes in California and Nevada. While a number of studies of
46 the Accelerating Moment Release (AMR) hypothesis have reported positive results, our
47 study is motivated by concerns that the existence of a number of free parameters in this
48 hypothesis could lead to false positive results if the effects of data-fitting are not
49 considered carefully. In particular, Bowman *et al.* [1998] adjust the region and time that
50 they inspect before each mainshock to optimize AMR, although theoretically, if a gradual
51 elastic build up of strain is the true cause of the acceleration, as claimed by Bowman *et al.*
52 [1998], the AMR signal should not be very sensitive to the space and time window.

53 Searching seismicity catalogs for precursors to large earthquakes has been an
54 active avenue of research for many years. This course of research is reasonable because
55 the obvious temporal and spatial clustering of earthquakes demonstrates that events
56 interact with each other. This line of inquiry is also appealing because earthquake
57 catalogs cover the entire globe, and, although their quality varies as both a function of
58 space and time, these catalogs are generally easy to obtain. However, it should be noted
59 that seismicity represents only part of the deformation processes involved in plate
60 tectonics and seismogenesis and thus provides only a limited view into possible
61 precursory behavior. Proposed seismicity precursors range from simple changes in the
62 rate of seismicity such as quiescence and activation, to those that include spatial patterns
63 such as Mogi-doughnuts [for overviews see Kanamori, 1981; Reyners, 1981], to complex

64 systems such as M8 [Keilis-Borok and Kossobokov, 1990] and Pattern Informatics
65 [Tiampo *et al.*, 2006].

66 Accelerating Moment Release is a more sophisticated version of the activation
67 hypothesis based on the concept that earthquakes are an example of a critical point
68 phenomena. According to the activation hypothesis one expects a precursory increase in
69 the rate of earthquakes before a large event. In the AMR hypothesis as formalized by
70 Bowman *et al.* [1998], the rate of seismicity increases such that the cumulative Benioff
71 strain (square root of the seismic moment or energy) [Benioff, 1951] follows a power-law
72 function until the time of an eventual mainshock. Thus it falls under the broad category
73 of seismicity rate changes. Reasenber and Matthews [1988] looked for rate changes
74 before 32 $M \geq 5.3$ earthquakes in central California (from 1974 to 1986) and Japan (from
75 1926 to 1984). If the statistics of each of the 32 sequences they studied are considered
76 separately, then they found statistically significant (at the 90% confidence level)
77 activation before 4 of the sequences, statistically significant quiescence before 3 of the
78 sequences, and no significant rate changes before the remaining 25 sequences. Thus if
79 each sequence were considered as an individual case study, 7 of them could contribute to
80 the literature on either activation or quiescence. However, taken as an ensemble the
81 result is clearly that there is no consistent, precusory pattern of seismicity rate changes
82 before earthquakes. The lesson of Matthews and Reasenber [1988] is clear: case studies
83 are not sufficient and we must test such hypotheses by looking at an entire catalog of
84 data.

85 Given the results of Matthews and Reasenber [1988] it is reasonable to ask why
86 one should continue to study the possibility that there are precursory rate changes before

87 large earthquakes. There are two differences between AMR and the method used by
88 Matthews and Reasenberg. First, AMR quantifies the seismicity by the cumulative
89 Benioff-strain while Matthews and Reasenberg used the number of earthquakes over a
90 given magnitude. This difference is important if the magnitude-frequency relationship
91 has temporal variations so that the count of earthquakes over a given magnitude is not
92 proportional to the Benioff-strain. Temporal variations in the magnitude-frequency
93 relationship are certainly possible and some have argued that there are precursory
94 variations in the *b-value* from the Gutenberg-Richter relationship [Reyners, 1981]. The
95 second difference is that AMR hypothesizes a gradual change in the seismicity while
96 Matthews and Reasenberg used a method optimized for sudden changes in the rate.
97 While the method of Matthews and Reasenberg should detect clear examples of AMR, it
98 is possible that it could miss some borderline cases. Thus, it is reasonable to do a study
99 specifically of the AMR hypothesis.

100 Our study will focus on the AMR hypothesis as presented by Bowman et al.
101 [1998]. This frequently cited paper is an important underpinning to current research
102 because it clearly formalized the AMR concept into a testable hypothesis and introduced
103 tests to estimate the statistical significance of the results. These tests used synthetic
104 seismicity catalogs to determine how often AMR could be observed by random chance.
105 Thus, Bowman et al. [1998] was an important step forward. Our study is motivated by
106 concerns that their tests may have underestimated the importance of data-fitting by
107 treating each mainshock in isolation (rather than considering a complete catalog of
108 events) and lacked sufficient statistical power because too few sequences were analyzed.

109 Also, Bowman et al. [1998] tested their results using synthetic catalogs that did not
110 include spatiotemporal clustering.

111 To test the AMR hypothesis, we first investigate the effects of data-fitting by
112 searching for both AMR and decelerating moment release (DMR) in both the California-
113 Nevada catalog and before the 2004 M9.3 Sumatra-Andaman Islands earthquake.
114 Second, we compare the frequency of AMR before large earthquakes in the actual
115 California-Nevada earthquake catalog with results obtained using synthetic seismicity
116 catalogs that contain no AMR. Multiple methods will be used to synthesize these
117 catalogs to ensure that the results are robust and not dependent on details of how the
118 synthetic catalog is produced. Third, we test the stability of scaling relationships between
119 the duration and spatial extent of apparent AMR patterns and the magnitude of the
120 earthquakes that follow.

121 Our tests are much more rigorous than the tests in Bowman et al. [1998] and other
122 AMR literature in several ways. Most importantly, we analyze the real data and
123 synthetics identically, which has not been done in any prior study of AMR. The data and
124 synthetics must be treated exactly the same, so that any differences in the observed AMR
125 behavior are clearly differences in the catalogs rather than differences in the analysis. In
126 order to make sure that the analysis is done uniformly, we use clearly defined search
127 parameters and avoid ad-hoc decisions when determining the amount of AMR in the data
128 and synthetics. We also compare AMR in the real catalogs with AMR in synthetic
129 catalogs containing realistic spatial-temporal clustering and multiple mainshocks.
130 Synthetics used in prior work have considered only one mainshock, and have not
131 included earthquake clustering.

132 In the years since Bowman et al. [1998] was published, various authors have
 133 proposed changes to the AMR method. Thus, if we focus only on Bowman et al. [1998]
 134 our conclusions could be outdated. For instance, Bowman et al. [1998] searched for
 135 AMR within circular regions around the large earthquakes. Bowman and King [2001]
 136 introduced search regions based on the Coulomb stress transfer pattern from a backslip
 137 model of the mainshock, based on the hypothesis that AMR would occur in the regions
 138 that are being loaded by the deformation that loads the mainshock fault plane. The utility
 139 of this hypothesis was tested using California seismicity by Mignan et al. [2006a] and we
 140 will further examine this hypothesis. Mignan et al. [2006a] also used declustered
 141 earthquake catalogs to try to reduce the effect of clustering and we will test whether or
 142 not this affects the statistical significance of the results. By doing so we ensure that our
 143 conclusions are applicable to the current state of the art.

144

145 3. Methods of Measuring AMR and Statistical Significance:

146

147 Bowman et al. [1998] formalized the search for AMR by developing a measure of
 148 whether the cumulative Benioff strain before an earthquake is better fit by a power-law
 149 function or a linear function with respect to time (Figure 1). The cumulative Benioff
 150 strain, $\varepsilon(t)$, is determined for a given radius around, and during a time period before, a
 151 mainshock:

$$152 \quad \varepsilon(t) = \sum_{i=1}^{N(t)} E_i(t)^{1/2} \quad (1)$$

153 where E_i is the energy of the i th event at time t and $N(t)$ is the number of events up to
 154 time t . We assume that $\log_{10}(E)$ is proportional to 1.5 times the magnitude (e.g.
 155 Kanamori and Anderson [1975]) but our results do not depend on the specific empirical
 156 relationship.

157 Two temporal functions are then fit to the cumulative Benioff strain curve: a linear
 158 function and a power-law function. The power-law function is:

$$159 \quad \varepsilon(t) = A + B(t_c - t)^m \quad (2)$$

160 where t_c is the time of the mainshock, B is negative, and $0 < m < 1$ for the power-law to
 161 be concave upward. To fit equation (2) to equation (1), the parameter A is set to the
 162 cumulative Benioff strain at the time of, and including, the mainshock.

163 Finally, to produce a measure of the degree of AMR before a mainshock, Bowman et
 164 al. [1998] introduced the parameter C :

$$165 \quad C = \frac{\text{power law fit root - mean - square error}}{\text{linear fit root - mean - square error}} \quad (3)$$

166 If the power law fits the observed cumulative Benioff strain better than the linear
 167 function, C will be less than 1. Bowman et al. [1998] require $m \leq 0.8$ so that the power-
 168 law function will not approximate a linear function. If the power-law function does not
 169 fit the data as well as the linear function, C will be greater than 1.

170 The C -value depends on the earthquakes used to determine $\varepsilon(t)$ and the earthquakes
 171 used depend on the size of the region selected around the mainshock, the time period
 172 before the mainshock, the magnitude range used to select the data, and the minimum
 173 number of earthquakes required to define a pattern. The magnitude range used by

174 Bowman et al. [1998] is 2 units smaller than the mainshock except when they concluded
175 that the catalog was complete to a lower level. Because such ad-hoc decisions cannot be
176 automated we will use the magnitude range of 2 units smaller than the mainshock. The
177 region around the mainshock is determined by adjusting the radius of the region until the
178 minimum C value is obtained, although Bowman et al. [1998] do not use a uniform
179 search criteria. Bowman et al. [1998] do not discuss how the time period used before
180 each mainshock is chosen, but since the amount of time used before each mainshock
181 varies, presumably these time periods have also been optimized to maximize AMR. We
182 want to essentially follow the protocol of Bowman et al. [1998] but wish to make the
183 optimization procedure more uniform so that our results are readily reproducible. We
184 find that we get very similar results to those of Bowman et al. [1998] if we use an
185 optimization method of varying the radius of the region around the mainshock from 20
186 km to 1000 km in steps of 20 km, and varying the start time before the mainshock from
187 the beginning of the catalog to the year before the mainshock in steps of 1 year.

188 Another issue is whether C varies with the minimum number of earthquakes required
189 for calculating an AMR solution (N_{min}). Bowman et al. [1998] note that acceleration
190 cannot be measured with fewer than 4 earthquakes and set $N_{min} = 4$. Mignan et al.
191 [2006a] use $N_{min} = 5$. Bowman (personal communication) has suggested, however, that
192 spuriously low C values might be calculated when data sets of earthquakes are very small
193 and has suggested $N_{min} = 10$. We measure how C varies in the real catalog when we use
194 N_{min} values of 4, 6, 8, and 10. We observe a small increase in mean C when N_{min} is
195 increased from 4 to 8. The values for $N_{min} = 8$ and $N_{min} = 10$ are the same, but with a
196 larger sample we might observe a difference. Thus to be conservative we do all of our

197 comparisons between the synthetics and real data using both $N_{min}=4$, in accordance with
198 Bowman et al. [1998], and $N_{min}=10$, in accordance with Bowman's later advice.

199 Bowman et al. [1998] define a successful AMR detection if $C \leq 0.7$, while other studies
200 [e.g. Mignan *et al.*, 2006b] use different threshold values of C . When we do our tests we
201 look at the full distribution of C values for a catalog of mainshocks, so that we are
202 sensitive to the full range of apparent AMR behavior.

203 We present the distributions of C -values for the real and synthetic data as cumulative
204 density functions (CDFs). If the real catalog exhibits more distinct accelerations than the
205 synthetic catalogs, the distribution for the real data should be larger for smaller values of
206 C than the distribution for the synthetics. Then, in the plots, the CDF curve for the real
207 data should lie above and to the left of the CDF curve for the synthetics. To visually
208 estimate the uncertainty in these CDFs, we also plot the 95% confidence regions of the
209 cumulative density functions as determined by bootstrap resampling of the distributions.
210 The bootstrap resampling assumes that the individual C -values are independent, although
211 in reality they are not because the data-selection regions for multiple mainshocks can
212 overlap. Thus, the bootstrap resampling slightly underestimates the true variability in the
213 CDFs and thus this visual representation may make the distributions of the real and
214 synthetic data look more distinct than they actually are.

215 Finally, we use a Kolmogorov-Smirnov (K-S) test to test the null hypothesis that the
216 distribution of C for the real mainshocks is not biased toward lower values of C than the
217 distribution of C for the synthetic mainshocks. Because the distribution of C for the
218 synthetic mainshocks is an observation with uncertainty, this K-S test is done as a two-
219 sided test. Because we test whether the real distribution is biased in one direction from

220 the synthetic distribution it is a one-tailed test. We present the results of this test as the
221 confidence that we can reject the null hypothesis. When this confidence is over 95% we
222 accept that more AMR is present in the real data than in the synthetic catalogs. Note that
223 the K-S test also assumes that the individual C -values are independent and thus also
224 slightly overestimates the statistical significance of AMR in the real data. Therefore our
225 tests are conservative with respect to falsely rejecting the AMR hypothesis and could
226 accept it even when it should be rejected.

227

228 4. Data

229 When we search for AMR before real earthquakes we use the ANSS catalog for
230 California and Nevada, available from the Northern California Earthquake Data Center
231 (www.ncedc.org/anss, last accessed on March 27, 2006) for the time period from 1950 to
232 2005. We define the California and Nevada region as from 31.5° to 42° N and 114° to
233 124° W (Figure 2).

234 Bowman et al. [1998] studied the 8 $M \geq 6.5$ earthquakes occurring after 1950 in
235 California as well as the 1986 M_L 5.6 Palm Springs earthquake and 3 smaller and larger
236 global earthquakes. This is a very small data set with which to do statistical tests since, as
237 we will show later, it is so easy to find apparent AMR signals in random data sets.
238 Bowman et al. [1998] only used mainshocks in California, although Nevada was part of
239 their study region and they included Nevada seismicity in their searches for AMR. No
240 reason is given for the lack of Nevada mainshocks, so we add in mainshocks located in
241 Nevada. A number of papers have claimed to observe AMR world-wide, and the smaller
242 Nevada earthquakes are already included in the analysis so there are no additional

243 concerns about catalog coverage or completeness, so including Nevada mainshocks
244 should not influence our results. This increases our sample size to 15 $M \geq 6.5$ mainshocks,
245 but this is still a very small sample.

246 One important question is how large an earthquake has to be to qualify as a
247 “mainshock”. We can increase the sample size by including smaller earthquakes as
248 mainshocks, but only if we can demonstrate that the degree of acceleration before our
249 new mainshocks matches what is seen before the $M \geq 6.5$ events. When Bowman et al.
250 [1998] analyze smaller events they caution that for smaller mainshocks the seismic
251 acceleration might be obscured by stress redistribution from larger earthquakes. We
252 evaluate whether it is possible to drop our mainshock magnitude to $M 6$ by calculating C
253 values before 42 $M \geq 6$ California/Nevada earthquakes. After eliminating two mainshocks
254 with C values that are >1 , one of which was $M > 6.5$, we measure the linear correlation
255 coefficient between mainshock magnitude and C . We find no significant correlation (the
256 linear correlation coefficient, r^2 , is 0.02 for the 40 earthquakes), indicating that lowering
257 the mainshock magnitude to $M 6$ does not change the AMR behavior of the sample.
258 Using even smaller mainshocks could improve our statistics further but would require us
259 to use earthquakes smaller than $M 4$ to search for the AMR, which would dip below the
260 magnitude completeness threshold of the 1950-2005 catalog.

261 The final step in our data selection is that we limit our entire earthquake catalog to be
262 post-1950. Bowman et al. [1998] also use primarily post-1950 data, but for the 1952
263 Kern County and 1989 Loma Prieta earthquakes they go back to 1910 to search for
264 acceleration. Bowman et al. [1998] do note that this can be problematic, as one expects
265 to see apparent seismicity rate accelerations from 1910-1949 due to improved detection

266 of earthquakes. Routine and consistent magnitude determination began in Southern
267 California in 1932 and in Northern California in 1948 [Uhrhammer *et al.*, 1996].
268 Bowman *et al.* [1998] attempt to correct for this by using only $M \geq 5.5$ earthquakes from
269 this period, but the statewide completeness magnitude was actually $> M 6$ [Toppozada
270 and Branum, 2002], or as large as the mainshocks themselves, and magnitude errors were
271 high. Further significant improvements to the seismic network in the 1970s and late
272 1990s may also create artificial acceleration in the catalog, but to a lesser extent since in
273 many areas of the state the improvement affected detection of earthquakes smaller than
274 the $M \geq 4$ shocks that we use here.

275 We find that starting the catalog in 1950 rather than 1910 does not bias our results
276 against the AMR hypothesis. AMR can be found before the Loma Prieta earthquake
277 without going back to 1950. For the 1952 Kern County earthquake it is true that a low C
278 value cannot be found using only post-1950 data. If true acceleration was occurring
279 before this earthquake it seems odd that it should not be apparent in the two years
280 immediately preceding the mainshock. Nonetheless we find that we can simply remove
281 the Kern County earthquake from the data base without affecting our statistical results.

282 We also note that extending the catalog back in time for some, but not all earthquakes,
283 is a form of special pleading (changing the rules for specific cases with no set guidelines)
284 and this makes it difficult to do a proper statistical test because one would have to
285 consider the special pleading for each of the mainshocks in the synthetic data sets. The
286 one exception we make is for our DMR tests (see below), for which we do go back to
287 1910 for the Kern County earthquake. However, the DMR tests are done to demonstrate
288 the power of data-fitting and we do not make statistical tests of these results.

289

290 5. Decelerating Moment Release and the Power of Data-fitting

291 The value of C is highly sensitive to the search radius (Figure 3). Increasing the radius
292 adds spatial clusters of earthquakes that may contribute to or counteract AMR, and C
293 changes accordingly. C is also sensitive to the catalog starting time. Temporal clusters of
294 events near the end of the catalog contribute to AMR, while those near the beginning
295 counteract it. Because C is unstable with respect to search radius, we hypothesize that
296 low C may be found in datasets with no true AMR, and therefore apparent AMR may be
297 the result of data-fitting.

298 The power of data-fitting to find any desired seismicity pattern can be demonstrated
299 by searching for a different pattern, for example a deceleration of seismicity rate, prior to
300 the same mainshocks that are cited as being preceded by AMR. If significant decelerating
301 moment release (DMR) is found before many of the mainshocks cited as examples of
302 AMR, then the most plausible explanation is that both patterns are the result of data-
303 fitting.

304 Searches for DMR require just two changes to the use of equation (2). First the
305 restriction $m \geq 1$ is applied to produce curves that are concave downward. Second, A is
306 left a free parameter because fixing it to the cumulative Benioff strain, including that of
307 the mainshock, would destroy any apparent deceleration. We then use the same
308 parameter C to measure the strength of the DMR.

309 To find DMR we first study the eight $M \geq 6.5$ California mainshocks for which
310 Bowman *et al.* [1998] reported AMR, and we use the same earthquake catalog to search
311 for these seismicity trends. DMR is found before all 8 mainshocks, and in each case the

312 DMR is significant according to Bowman *et al.* [1998]’s criteria of $C < 0.7$ (Figure 4).
313 The optimal radii and time windows are similar to those for AMR, so AMR and DMR are
314 not characteristic of different length or time scales (Table 1).

315 We next search for both AMR and DMR before all $M \geq 6$ mainshocks that occurred
316 after 1950 in the ANSS catalog for California and Nevada. Figure 5 shows the
317 cumulative distribution of the observed curvature parameter C for the optimal AMR and
318 DMR before each mainshock. Although the C value distributions for AMR and DMR are
319 not directly comparable statistically because of the difference in whether A is fixed or
320 treated as a free parameter, it is clear that there are nearly as many mainshocks with well-
321 resolved DMR signals (low C) as with well-resolved AMR signals. Many mainshocks
322 exhibit both AMR and DMR for different data-selection choices.

323 Another example of data-fitting is for the December 2004 $M 9.3$ Sumatra earthquake.
324 Two studies [Jiang and Wu, 2005; Mignan *et al.*, 2006b] report significant AMR prior to
325 this event beginning around 1980. Following Mignan *et al.* [2006b], we use shallow
326 events ($\text{depth} \leq 40$ km) from the ANSS global earthquake catalog from 1965-2004
327 (www.ncedc.org/anss, last accessed on February 16, 2007). We consider a catalog
328 containing all events $M \geq 4.5$, and, because the $M \geq 4.5$ catalog is clearly not complete (see
329 Mignan *et al.* [2006b] Figure A1), we also consider a catalog containing all $M \geq 5.5$
330 events. While Mignan *et al.* [2006b] search for AMR in regions based on Coulomb stress
331 modeling, we search for AMR and DMR using circular regions. We show in Section 6.3
332 that the difference in region shape does not make a significant difference in the
333 identification of AMR for California and Nevada.

334 Both significant AMR and significant DMR ($C < 0.7$) are found in the pre-Sumatra
335 earthquake catalogs (Figure 6). The optimal AMR curve for the $M \geq 4.5$ catalog (Figure
336 6(a)) is similar to the curve of Mignan *et al.* [2006b], verifying that the difference in
337 region shape is not greatly important. The C -value for the $M \geq 4.5$ DMR curve is
338 somewhat higher than for the $M \geq 4.5$ AMR curve, which is probably the result of the
339 incompleteness of the $M \geq 4.5$ catalog. An incomplete catalog will become more complete
340 through time, producing an artifact of apparently increasing seismicity rate. For the more
341 complete $M \geq 5.5$ catalog, the C -values for the optimal AMR and DMR curves are more
342 similar. The optimal AMR curves begin around 1980, while the optimal DMR curves
343 begin around 2000. Much of the data-fitting in the Sumatra case depends on two $M 7.9$
344 events occurring in June 2000 (one in Sumatra, one in the Indian Ocean.) If these events
345 occur near the end of the selected time window, apparent AMR is observed, while if
346 these events occur near the beginning, apparent DMR is observed. Note that the AMR
347 and DMR curves contain a similarly large number of events, so no argument can be made
348 that the AMR curve is more real based on the large number of events that define it.

349 There is no significance to the longer time-scale of apparent AMR than DMR for the
350 Sumatra example. For the eight California events studied by Bowman *et al.* [1998], the
351 optimal time-scales and length-scale for DMR overlap with those for AMR (Table 1.)
352 One example of an earthquake with a longer time-scale of apparent DMR is the 1971 San
353 Fernando earthquake. Optimal DMR is found starting in 1950 (Figure 4, Table 1) while
354 optimal AMR starts in 1967 (see Figure 6 of Bowman *et al.* [1998]) In this case, the
355 data-fitting involves a period of low seismicity rate during 1956-1968. If the selected
356 window begins during this time, apparent AMR is observed, while if this time occurs

357 later in the time window, apparent DMR is observed. This example and the Sumatra
358 example demonstrate how fluctuations in the background seismicity rate can be selected
359 to produce the desired seismicity pattern.

360 None of these examples should be taken to imply that DMR is a real precursory
361 process. Instead, these examples demonstrate that two contrary signals, accelerating and
362 decelerating seismicity, can often be found in the same dataset. It seems implausible that
363 true acceleration and deceleration are simultaneously present, strongly suggesting that
364 both signals are found as a result of data-fitting.

365

366 6. Synthetic Seismicity Tests

367 We further consider the possibility that AMR is not a real physical process, and that it
368 is found before many mainshocks because the time and area windows are adjusted to
369 optimize for acceleration. If this explanation is correct, AMR should be found at a
370 similar rate in real catalogs and in synthetic catalogs in which no real AMR is present.
371 We perform this test by generating suites of synthetic catalogs and searching them for
372 AMR in the same way as the real catalogs. The null hypothesis is that the synthetic
373 catalogs contain as much AMR as the real catalog. A rejection of this null hypothesis
374 would support AMR as a real physical phenomenon. If the null hypothesis cannot be
375 rejected, this would support our theory that AMR is an artifact of data fitting. As
376 discussed in the Methods section, we use the 95% confidence level as the test of whether
377 or not the null hypothesis can be rejected.

378

379 6.1 Synthetic Seismicity Catalogs

380

381 We generate four types of synthetic test catalogs using different approaches. These
382 catalogs range from purely random earthquake times and locations to more complex
383 catalogs based on two ETAS (epidemic-type aftershock sequence) models [e.g. Ogata,
384 1988] that include both realistic spatiotemporal earthquake clustering and a realistic
385 spatial distribution of background seismicity. Each synthetic catalog is designed to
386 contain approximately the same number of events as the real catalog, and to span the
387 same spatial area and duration.

388

389 6.1.1 Uniform Random Seismicity Catalogs

390

391 The first type of synthetic catalog is the simplest, consisting of uniform random
392 seismicity. The number of events in each synthetic catalog matches the number in the
393 real ANSS CA-NV catalog. The synthetic event locations and times are randomly
394 selected from a uniform distribution over the spatial and temporal range of the real ANSS
395 catalog. The magnitudes are selected randomly, without replacement, from the
396 distributions of magnitudes in the real catalog. We generate 10 simulated catalogs in this
397 way, for a grand total of 420 mainshocks. This method produces synthetic seismicity that
398 matches the number of earthquakes and the magnitude distribution from the real catalog
399 but does not produce realistic spatial or temporal clustering behavior (Figure 7c and d).

400

401 6.1.2 Random Times/Real Locations Catalogs

402

403 The next type of synthetic catalog more resembles real seismicity in that it contains the
404 same spatial clustering as the real data. The real earthquake locations are used, while the
405 synthetic earthquake times and magnitudes are assigned randomly as before. Again we
406 generate 10 simulated catalogs in this way, containing a total of 420 mainshocks. This
407 method produces synthetic seismicity that matches the number of earthquakes, magnitude
408 distribution, and spatial pattern of the real catalog but does not include realistic temporal
409 clustering (Figure 7e and f).

410

411 6.1.3 ETAS Synthetic Seismicity Catalogs

412

413 The third and fourth sets of synthetic catalogs consist of ETAS simulations [e.g. Ogata,
414 1988] that include realistic spatiotemporal earthquake clustering (Figure 7g-j). The times
415 of the background earthquakes are chosen randomly, using a spatially-varying (on a 0.5°
416 grid) background seismicity rate found from the real ANSS catalog using the technique
417 of Hainzl *et al.* [2006]. For the magnitude distribution for the third set of simulations we
418 assign the magnitude of each earthquake randomly from the Gutenberg-Richter
419 distribution with a b value of 1.0, following Felzer *et al.* [2002]. For the fourth set of
420 simulations we choose magnitudes randomly from the magnitudes listed in the ANSS
421 catalog. Note that the total number of earthquakes in each ETAS simulation and in the
422 ANSS catalog will not necessarily be the same, and thus some magnitudes will be
423 randomly omitted or repeated.

424 Our synthetic ETAS catalogs do not exactly match the number of earthquakes in the
425 original catalogs, or the sharpness of the fault system, but do produce realistic spatial and

426 temporal clustering. For the purposes of this study, we believe that these catalogs are
427 adequate. Further details on the ETAS simulations are presented in the Appendix.

428

429 6.2. Synthetic Seismicity Results

430 The cumulative density functions (CDF) of the C -values for the real data and the
431 synthetic catalogs are shown in Figure 8. The CDF curves, with the 95% confidence
432 regions estimated using a bootstrap approach, provide a visual comparison between the
433 results from the real data and the synthetic catalogs while the statistical significance
434 estimated using a K-S test provides an objective measure of whether or not the null
435 hypothesis (that the real catalog does not produce more AMR than the simulated
436 catalogs) can be rejected.

437 It is clear that increasing N_{min} has only a small effect on the results. Higher N_{min} does
438 increase the statistical significance of AMR but in no case does the difference between
439 $N_{min} = 4$ and $N_{min} = 10$ change whether or not the null hypothesis can be rejected. For
440 most mainshocks, the number of events in the optimal sequence, N , is greater than N_{min}
441 (Figure 9(a).) Low values of C arise in sequences with a range of values of N , and hence
442 are not an artifact of small datasets (Figure 9(a).)

443 However, whether or not we reject the null hypothesis is dependent on whether or not
444 the synthetic catalogs contain spatiotemporal earthquake clustering. The CDFs for the
445 two types of synthetic catalogs without spatiotemporal clustering, the uniform random
446 seismicity and the randomized earthquake catalog, show significantly less AMR than the
447 CDF for the real data at above 95% confidence. For the two ETAS simulations, which

448 contain realistic spatiotemporal clustering, we cannot reject at 95% confidence the null
449 hypothesis that the CDFs for the synthetics contain as much AMR as the CDF for the real
450 data.

451 The cumulative distribution curves for the real and ETAS catalogs exhibit a steep
452 slope starting at $C \approx 0$, indicating that both datasets include mainshocks preceded by
453 distinct and well-resolved accelerations with small C . The CDFs for the synthetic
454 datasets without spatiotemporal clustering have a shallow slope for very small values of
455 C and become steep only for larger values of C , indicating that few of the non-ETAS
456 synthetic mainshocks are associated with AMR with very small (less than ~ 0.2) C values.

457 The rate and strength of AMR observed in real and ETAS seismicity catalogs is the
458 same, despite the fact that no real AMR exists in the ETAS catalogs. The spatiotemporal
459 seismicity clustering contributes to the apparent AMR, because each earthquake may
460 become a foreshock by directly or indirectly triggering a mainshock. When the rate of
461 seismicity is higher than usual, the probability of a mainshock being triggered is also
462 higher and this may look like AMR. We conclude that AMR is observed before many
463 mainshocks both because of the clustering process and because a search is done for the
464 spatial and temporal extent of the region that optimizes the AMR signal.

465

466

467 7. Scaling Relationships

468 The size of the region over which AMR is observed has been reported to scale with
469 the magnitude of the eventual mainshock [e.g. Bowman *et al.*, 1998]. This apparent
470 scaling is often used as an argument in support of AMR as the result of a real physical

471 process, since a critical region of increased loading would reasonably scale with the size
472 of the eventual rupture. The time period over which AMR is observed also appears to
473 scale with mainshock magnitude in their results.

474 We first investigate the robustness of the proposed scaling relationship between
475 mainshock magnitude and the size of the region exhibiting AMR. Bowman *et al.* [1998]
476 proposed a linear scaling relation between the log of the optimal region size and
477 mainshock magnitude based on 8 $M \geq 6.5$ California mainshocks, and 4 additional
478 earthquakes that extend the magnitude range. For only 2 of the 8 California events,
479 however, does the confidence region for the optimal radius intersect the scaling
480 relationship curve (their Figure 7). We test for AMR for the same 8 California
481 mainshocks, using the radius scaling relation given by Bowman *et al.* [1998] and a
482 duration scaling relationship found from a linear fit of the log of the optimal duration
483 reported by Bowman *et al.* [1998] versus event magnitude (Figure 10b). Using catalogs
484 with spatial and temporal windows defined by these scaling relations, we find no
485 significant AMR ($C < 0.7$) for the 8 California mainshocks.

486 These results imply that the proposed scaling cannot be strictly applied, and in
487 particular cannot be used predictively to estimate the spatial or temporal region in which
488 AMR is expected to occur prior to a given mainshock or anticipated future earthquake.
489 The scaling relation isn't robust because apparent AMR is very sensitive to the radius and
490 duration of the catalog. The value of C can change dramatically over a small increase in
491 region size (Figure 3), as additional earthquake clusters are captured in the region,
492 changing the shape of the cumulative Benioff strain curve. Thus, while the optimal radii
493 and durations found by Bowman *et al.* [1998] roughly scale with magnitude, the

494 difference between the optimal values and the best-fit curve translates to a significant
495 difference in C -value. Therefore, the scaling relationships cannot be used to predict the
496 data-selection parameters and avoid the problems of data-fitting.

497 The apparent general increase in optimal region size (Figure 10a) and duration (Figure
498 10b) could still be used as an argument for a physical basis for AMR, even though
499 particular proposed scaling relationships don't strictly hold. We test whether this
500 apparent scaling is an artifact of data selection. Bowman *et al.* [1998] search for AMR
501 before each mainshock using a catalog with a minimum magnitude cutoff two magnitude
502 units below the mainshock magnitude. Using a minimum magnitude that scales with the
503 mainshock magnitude can affect the apparent optimal region size and AMR duration. For
504 a larger mainshock, because of the relative infrequency of larger events, there will be a
505 lower spatial and temporal density of events within two magnitude units, and hence a
506 larger area and/or a longer time period may be needed to accumulate enough events to
507 observe significant AMR. An apparent scaling of optimal region and duration with
508 magnitude could follow.

509 We examine the dependence of the apparent scaling on minimum magnitude using the
510 same 8 California mainshocks studied by Bowman *et al.* [1998]. First we find scaling
511 relationships using the optimal radii and durations reported by Bowman *et al.* [1998].
512 Because we do not include their additional 4 earthquakes (which would introduce more
513 data-selection issues concerning how these 4 events were chosen), we obtain a somewhat
514 different scaling relationship for radius versus magnitude, but still with a positive slope
515 (Figure 10a.) We also find a positive slope for the optimal duration versus magnitude
516 (Figure 10b). For these 8 events, optimal region size and duration weakly scale with

517 mainshock magnitude, when the optimization is performed on catalogs with a minimum
518 magnitude that scales with mainshock magnitude.

519 Next we find the optimal radii and durations for the 8 mainshocks using catalogs with
520 a fixed minimum magnitude of M 4.0. In this case, we find no positive correlation of
521 optimal region size or duration with mainshock magnitude. The fits to optimal radius
522 versus magnitude (Figure 10c) and optimal duration versus magnitude (Figure 10d) are
523 both essentially flat, with very small negative slopes. Similar results are obtained for
524 minimum magnitudes ranging from M3.0 (probably below the magnitude of
525 completeness) to M4.5 (within 2 magnitude units of the smallest mainshocks.) There is
526 no scaling of optimal region size or duration with mainshock magnitude when the
527 optimization is performed on catalogs with a fixed minimum magnitude. Therefore, the
528 apparent radius and duration scaling in this dataset is an artifact of using a minimum
529 magnitude that scales with mainshock magnitude, and should not be interpreted in terms
530 of physical processes.

531

532 8. Tests of Recent Changes in AMR Detection Efforts

533 In the years since Bowman et al. [1998] was published, several authors have proposed
534 methodological changes to make the search for AMR more effective.

535

536 8.1. Coulomb Prestress Regions

537 One important change is that while Bowman et al. [1998] searched for AMR within
538 circular regions around the large earthquakes, Bowman and King [2001] used search
539 regions based on the Coulomb stress transfer pattern from a backslip model of the

540 mainshock, based on the hypothesis that AMR would occur in the regions that are being
541 loaded by the deformation that loads the mainshock fault plane. This method was also
542 advocated by King and Bowman [2003], Mignan et al. [2006a], and Mignan et al.
543 [2006b].

544 The conceptual model is that the eventual mainshock fault patch remains locked, while
545 the rest of the fault slips aseismically at depth and in earthquakes on either side of the
546 locked patch. This is equivalent to modeling back-slip on the mainshock plane [e.g.
547 Savage and Burford, 1973]. Only events in areas of positive Coulomb stress change
548 (ΔCS) in the build up to the mainshock are considered when searching for AMR, down to
549 a minimum stress value ΔCS_{min} , which is chosen to optimize AMR. We test whether
550 using a region based on this hypothetical model of stress loading improves the
551 performance of the AMR model.

552 We model prestress for nine $M \geq 6.5$ mainshocks in the CA-NV ANSS catalog, using
553 simple mainshock slip models with uniform slip on a single fault plane, following
554 Bowman and King [2001]. We use published slip models for the San Fernando [Heaton
555 and Helmberger, 1979], Superstition Hills [Wald *et al.*, 1990], Loma Prieta [Wald *et al.*,
556 1991], Landers [Wald and Heaton, 1994], Northridge [Wald *et al.*, 1996], Hector Mine
557 [Ji *et al.*, 2002], and San Simeon [Ji *et al.*, 2004] earthquakes. We simplified the models
558 by creating a single fault plane of average strike and dip, and assigning uniform slip to
559 this plane to match the mainshock moment. To model the backslip we model slip in the
560 opposite direction from the mainshock slip model. For the Fairview Peak mainshock, we
561 use the surface rupture from Caskey *et al.* [1996] to determine the location, strike, and
562 length of the rupture, and the moment tensor of Doser [1986] to constrain the moment,

563 the fault dip and the rake. For the Borrego Mountain earthquake we use the surface
564 rupture reported by Allen *et al.* [Allen *et al.*, 1968] and the moment tensor of Ebel and
565 Helmberger [1982]. Because our tests require a minimum of 10 earthquakes before the
566 mainshock in both the full and positive prestress regions ($N_{min}=10$), we do not use the
567 Kern County, Rainbow Mountain, Stillwater, and Dixie Valley earthquakes, all of which
568 occurred early in the catalog.

569 We compute the static stress change tensor due to each mainshock backslip
570 dislocation, assuming an elastic half-space, using the computer program DLC (R. W.
571 Simpson, personal communication) based on the subroutines of Okada [1992]. We find
572 ΔCS on optimally oriented planes at the hypocenter of each earthquake in the ANSS
573 catalog occurring prior to the mainshock. The optimally oriented planes are found
574 assuming that the maximum compressive stress axis of the background stress field is at
575 45° to the fault plane and that the differential stress is 10 bars, following similar
576 assumptions made by Bowman and King [2001]. We also assume an effective
577 coefficient of friction $\mu=0.4$.

578 For each of the nine $M \geq 6.5$ mainshocks of the CA-NV ANSS catalog modeled above,
579 we first search for AMR and find the lowest value of C using only events inside the
580 positive prestress region with $\Delta CS \geq \Delta CS_{min}$. As a control, we then separately determine
581 the lowest value of C using earthquakes in both the positive and negative prestress zones
582 by selecting all events with $|\Delta CS| \geq \Delta CS_{min}$. We find the value of ΔCS_{min} that optimizes
583 the AMR by stepping through 100 different stress values for ΔCS_{min} between 0.0001
584 bars and the largest positive stress change modeled for the earthquake. As in our other
585 tests we find the optimal beginning time by stepping in 1-year increments. If AMR is a

586 real physical process that occurs primarily in the positive prestress zone, then the
587 earthquakes in the positive stress zones should produce a significantly lower C value than
588 the combined shadowed and positive stressed earthquakes. On the other hand, if AMR is
589 unrelated to prestress, for instance if AMR is an artifact of data fitting, the two C values
590 will be comparable.

591 We find that using the positive prestress region does not significantly improve the
592 performance of the AMR model. Limiting the data set to events with positive prestress
593 produced a lower value of C for only three of the mainshocks (Table 2.) For 5 of the
594 mainshocks, using all of the earthquakes produced a better result, and there was one tie.
595 Limiting the search for AMR to the positive prestress areas therefore does not
596 significantly improve the chances of finding AMR.

597

598 8.2. Fixed Curvature Parameter

599 The approach of Mignan *et al.* [2006a] also differs from our work and Bowman *et al.*
600 [1998] in two important aspects. First, while we followed Bowman *et al.* [1998] and
601 considered the exponent m in equation 2 as a free parameter allowed to range between 0
602 and 0.8, Mignan *et al.* [2006a] fixed it to $m = 0.3$ based on Bufe and Varnes [1993].
603 Constraining the exponent m reduces the power of data-fitting when fitting the power-law
604 to the data and very low C -values will only be found when the data exhibit power-law
605 type behavior with $m \approx 0.3$. This is equally true for the real data and the synthetic
606 catalogs, thus this modification would improve the statistical significance of the AMR
607 hypothesis if the m -exponents in the real data are actually about 0.3.

608 If the true value of $m \approx 0.3$, we would expect to see the values of m that optimize
609 AMR for the real data to cluster around 0.3. However, we do not find that m tends to be
610 about 0.3 in the real data, but rather spans the range of values (Figure 9(b).) It could be
611 argued that a larger catalog could more precisely determine m , but we find a wide range
612 of optimal m even for data sets with large N (Figure 9(c).) It is also interesting that the
613 lowest C -values correspond to very low m (Figure 9(d).) This may be an artifact of the
614 definition of C , because when m is very low the power-law is the most different from a
615 line.

616 When we constrain m to 0.3 and re-analyze the real data and the ETAS simulations,
617 very low C -values become more rare in both the real data and the synthetics. Setting
618 $m=0.3$ does not improve the statistical significance of the AMR hypothesis (Figure 11.)
619 For both $N_{min}=4$ and $N_{min}=10$, the null hypothesis, that the synthetic data contains as
620 much AMR as the real data, cannot be rejected with 95% confidence. Because our
621 results show that the m -values found in the real data do not cluster near 0.3 and
622 constraining m to 0.3 does not improve the statistical significance of the AMR signal, our
623 analysis of a larger data set than Bufe and Varnes [1993] rejects their hypothesis that m is
624 about 0.3.

625

626 8.3. Declustering

627 Second, Mignan et al. [2006a] declustered their earthquake catalogs (removed
628 aftershocks) before testing for AMR. The theory behind this change was that aftershocks
629 are not necessarily part of the AMR acceleration and so may detract from detection of the
630 underlying AMR signal. To test whether declustering improves the performance of the

631 AMR model we used the well known algorithm of Gardner and Knopoff [1974] to
632 decluster both the real ANSS catalog and ten synthetic ETAS catalogs, where the
633 synthetic catalogs were produced with magnitudes taken from the Gutenberg-Richter
634 distribution. We then performed new optimizations for AMR, solving for a new C value
635 for each mainshock that survived the declustering process. As could be expected from
636 our earlier analysis, declustering caused the overall incidence of low C values to
637 decrease. Furthermore the amount of decrease was similar in the CDFs for the real and
638 synthetic declustered catalogs, such that a K-S test using the CDFs based on the
639 declustered data cannot reject the null hypothesis that the C -values of the synthetic data
640 are as low as the C -values of the real data (Figure 12). Therefore we find no evidence of
641 the existence of real AMR being concealed by aftershock sequences.

642

643 9. Discussion

644 Determining free parameters from data is often a necessary part of hypothesis
645 development. Given the hypothesis that seismicity accelerates before large earthquakes,
646 it may be reasonable to determine the region and time period over which the acceleration
647 takes place from the data. In AMR studies this is done when the size of the region and
648 length of the time period are determined by minimizing the C -value for each earthquake.
649 This practice, frequently referred to as data-fitting, carries the danger of identifying
650 patterns that are not real, but are created by choosing the free parameters so that the
651 selected data demonstrates the hypothesized pattern. This danger is particularly high
652 when the results are unstable with respect to small variations in the free parameters.
653 Given that the C -value is an unstable function of the selection radius (Figure 3) and time

654 period, the dangers of data-fitting with respect to AMR must be carefully considered.
655 This instability also implies that the apparent AMR signals are not the result of a broad
656 regional process but are created by optimally selecting a series of spatial clusters that
657 create an apparent acceleration. The dangers of data-fitting are also illustrated by the fact
658 that contrary patterns of accelerating and decelerating moment release can be found in the
659 same, real, datasets by choosing selected radii or time periods.

660 One way to escape the dangers of data-fitting would be to determine these free
661 parameters by some other means. Bowman *et al.* [1998] proposed empirical scaling
662 relationships between the magnitude of the impending mainshock and the size of the
663 search region. However, we have demonstrated that this empirical relationship cannot be
664 used to avoid data-fitting because when it is used to determine the data-selection area
665 there is no AMR signal. Furthermore, we have demonstrated that this proposed scaling
666 relationship is due to the practice of using a minimum magnitude that scales with the
667 mainshock magnitude. Thus the proposed scaling relationships are a statistical artifact of
668 the design of the algorithm and are not evidence of a physical process.

669 Given the danger that spurious patterns may result from data-fitting, it is critical that
670 we test the statistical significance of AMR. We carry out these statistical tests by
671 creating simulated seismicity catalogs, subjecting these simulated catalogs to exactly the
672 same analysis as was applied to the real data, and then determining the probability that
673 the distributions of C -values for the real data are lower than the C -values for the synthetic
674 catalogs. In this study, we carry out this process using four types of seismicity
675 simulations that each serve to illustrate the important elements of these tests.

676 The first two seismicity simulations are very simplistic and do not include temporal
677 clustering. The first simulation method creates seismicity that has a random, uniform
678 distribution in time and space and magnitudes are drawn from the real catalog with the
679 rate set to match the rate of earthquakes in the real data. The second simulation differs
680 only in that it uses the locations from the real catalog and thus preserves the spatial
681 characteristics of real data. While many cases of AMR are found in these random
682 catalogs, more are found in the real data and the K-S test rejects the null hypothesis that
683 the synthetic catalogs contain as much AMR as the real catalog. Thus, using these simple
684 random catalogs would lead to accepting AMR as a real process. Our second two
685 seismicity simulations do include temporal clustering, however, in the form of
686 aftershocks modeled with an ETAS simulator. When this clustering is included the
687 amount of AMR in the real catalog is not statistically significantly greater than the
688 amount of AMR in the synthetic catalogs.

689 Important lessons can be drawn from a comparison between the results of our tests
690 using seismicity simulations with the tests done in Mignan *et al.* [2006a]. Their
691 simulations produce distributions of C -values where low C -values are rare compared to
692 both the real data and to our ETAS simulations. This is because their simulation methods
693 are most similar to our uniform random synthetic seismicity catalogs, which have events
694 uniformly distributed in space and time. But there are also important differences between
695 their methods and our simple synthetic tests. For instance, our synthetics more
696 realistically represent a full seismicity catalog that includes multiple mainshocks, while
697 their catalogs consider individual mainshocks in isolation. In their simulations, a cluster
698 of seismicity may only contribute to an AMR signal preceding one earthquake. In our

699 synthetic catalogs, as in real data, a cluster of seismicity exhibiting a rate increase may
700 contribute to the apparent AMR of multiple mainshocks, making apparent AMR more
701 common. Mignan et al. [2006a] attempt to compensate for the lack of clustering in their
702 simulations by declustering their data. However, declustering algorithms are imperfect
703 and so are unlikely to produce a truly uniform catalog in both space and time. Also, the
704 number of earthquakes in their simulations is set to an artificial number in a non-
705 dimensional space rather than basing the simulations on the number of earthquakes in the
706 actual catalog with the same spatial size and temporal duration as the real data. Thus the
707 approach Mignan et al. [2006a] does not generate a realistic simulation of the actual data
708 analysis process and this is one of the deficiencies that leads them to underestimate the
709 rate at which low C -values will be found by random chance.

710 Bowman *et al.* [1998] also test the AMR they find against AMR in synthetic catalogs
711 but like Mignan et al. [2006a] their synthetics have no spatiotemporal clustering and
712 contain only one synthetic mainshock per catalog. Most critically, however, Bowman *et*
713 *al.* [1998] also evaluate their synthetics differently than the real data; whereas the time
714 windows are apparently optimized for the real mainshocks and the minimum magnitude
715 is sometimes adjusted, a uniform time window and magnitude range are used for the
716 synthetics. As a result the C values for the synthetics produce a very different CDF than
717 is found in either this study or in Mignan et al. [2006a].

718 The problems associated with not acknowledging that earthquakes may be part of the
719 AMR for multiple mainshocks in the real catalog is also compounded in Bowman *et al.*
720 [1998]. From their simulations, Bowman *et al.* [1998] find that the probability of
721 obtaining a C -value below 0.7 is 0.5 and then calculate the probability of finding 8 C -

722 values below 0.7 by assuming that the C -values are independent. This makes the joint
723 probability of obtaining 8 C -values below 0.7 equal to 0.5^8 and makes their result for the
724 real data appear to be significant at over the 99% confidence level. In fact, because the
725 seismicity catalog is shared between all of the earthquakes, if one C -value less than 0.7 is
726 found then the chances are very good that other like values will be found as well. Thus,
727 the C -values in the real data are not independent and their approach overestimates the
728 statistical significance of the signal.

729 The next two simulation methods we use include realistic spatiotemporal clustering
730 and the general spatial characteristics of the real data. The difference between the two
731 simulations is that one uses a Gutenberg-Richter distribution to produce the magnitudes
732 while the other uses an empirical distribution drawn from the real data. The simulation
733 methods with clustering, as compared to those without clustering, produce distributions
734 of C -values that are even more similar to the one from the real data. Thus, when
735 clustering is included the K-S test rejects the AMR hypothesis. The effect of including
736 clustering in the test is similar to the conclusions of Michael [1997] who studied the
737 effect of seismicity clustering on a proposed electromagnetic precursor. This is because
738 clustering, which exists in real data, can help artificial data-fitting find unusual behavior.
739 Therefore it is always important to include the effects of clustering in prediction tests.
740 The synthetic catalogs of Bowman *et al.* [1998] and Mignan *et al.* [2006a] do not include
741 spatiotemporal clustering, leading to poor simulation of C -values in their synthetic tests.
742 The fact that only our ETAS simulated catalogs matched the amount and distribution of
743 AMR seen in the real catalog may also indicate, perhaps not too surprisingly, that the

744 sudden rate increases occurring in aftershock and foreshock sequences of all sizes may
745 accentuate apparent accelerations.

746 We have found that spatio-temporal clustering in the form of aftershock sequences
747 significantly increases the amount of apparent AMR that is found in a data set. One or
748 several large aftershock sequences might lead to both a stronger apparent AMR signal
749 and an increased chance of a large earthquake simply because larger earthquakes are
750 more likely to occur during times of higher seismicity rates. This is because the higher
751 the earthquake rate, the higher the probability of at least one large earthquake. Thus the
752 existence of clustering makes AMR appear to be predictive. However, if the physical
753 factor producing the apparent acceleration is aftershock clustering, forecasting of the
754 probability of large earthquakes can be accomplished by existing applications of
755 aftershock statistics via an ETAS [Helmstetter *et al.*, 2006] or STEP [Gerstenberger *et*
756 *al.*, 2005] type model.

757 We have focused on the AMR hypothesis as originally proposed in Bowman *et al.*
758 [1998] rather than in one of many later studies that have proposed modifications in the
759 hypothesis. One major change came when Bowman and King [2001] proposed using
760 data selection regions based on Coloumb stress changes rather than circles around the
761 impending mainshock. By comparing the distribution of C -values found for the circles
762 and stress patterns in the real data, we show that this modification does not result in an
763 improved AMR signal.

764 This result is in contrast to those of Mignan *et al.* [2006a], who report lower values of
765 C in positive prestress regions than in negative prestress regions. Their methodology was
766 to determine the optimal circular area, and then to compare the positive and negative

767 prestress regions within the optimal circle. However, the positive prestress region fills a
768 larger portion of the circle than the negative prestress region (see their Figure 5), so the
769 optimization of AMR in the circular area is weighted towards optimizing AMR in the
770 positive prestress region, biasing the result. For 2 of the 9 mainshocks, the negative
771 prestress region inside the circle is so small that it contains <5 events. Further bias is
772 introduced by assigning a value of $C=1$ to the negative regions when less than 5 events
773 are present, which guarantees that the positive pre-stress region will have a lower C
774 value. Our tests do not contain this bias, since we optimize the positive prestress catalog
775 and the whole catalog independently.

776 There are many other proposed modifications and it is outside the scope of this study
777 to examine each of them. Instead, the original authors should subject their proposals to
778 rigorous statistical tests as we did for Bowman *et al.* [1998]. In addition to fully
779 simulating the analysis process and using realistic simulations of the seismicity, including
780 clustering, these tests must include a large data set so the tests have sufficient statistical
781 power. Case studies of individual events, or even several events, may be useful when
782 developing a hypothesis but are inadequate for testing purposes.

783

784 10. Conclusions

785 We have shown that apparent AMR in California and Nevada results from a
786 combination of data-fitting and the spatiotemporal clustering of earthquakes. We
787 compared real data with synthetic datasets containing no underlying AMR, including
788 ETAS simulations with realistic spatiotemporal clustering of earthquakes, and found the
789 rate and strength of AMR in the real and ETAS catalogs to be indistinguishable. The

790 high rate of observed AMR in all types of synthetic simulations demonstrates how easily
791 apparent AMR can be found by optimizing the spatial and temporal windows. Proposed
792 scaling relationships, which could help avoid artifacts of data-fitting, have turned out to
793 be both unstable and a statistical artifact of using a minimum magnitude that scales with
794 the mainshock magnitude.

795 The difference between the amount of AMR found in random simulations and real
796 data on one hand, and the similar amount found in the ETAS synthetics and real data on
797 the other, demonstrates the contribution of spatiotemporal earthquake clustering to
798 apparent AMR. Observed AMR therefore doesn't imply any new earthquake behavior or
799 physics, beyond the known occurrence of aftershocks and foreshocks. AMR
800 consequently has no more predictive power than clustering-based forecasts [e.g.
801 Gerstenberger *et al.*, 2005; Helmstetter *et al.*, 2006; Reasenber and Jones, 1994;
802 Reasenber and Jones, 1989]. The clustering-based methods are preferable because they
803 parameterize the earthquake clustering more directly.

804 Our study focused on AMR as defined in Bowman *et al.* [1998], the foundation of
805 most current AMR research. We also explored several more recent modifications,
806 including spatial regions based on stress loading, removal of aftershocks before searching
807 for AMR, and constraining the curvature parameter (m) to 0.3, and demonstrated that
808 these modifications do not change the results. Other modifications to AMR are of course
809 possible, and our study provides a model for testing any revised definition of AMR. In
810 particular, if there is any true signal, it should be significantly stronger in real data than in
811 ETAS simulations

812 Our results also have broader implications for the interpretation of other observed
813 seismicity patterns. The spatiotemporal clustering of earthquakes makes it easy to find a
814 desired pattern of seismicity rate changes, especially when there are adjustable
815 parameters. For example, we found AMR in most random synthetic catalogs, and also
816 found two conflicting patterns of acceleration and deceleration in many of the same real
817 datasets. Similarly, other parameterizations of activation or quiescence, or more complex
818 patterns, may also be easily found.

819 Because a particular seismicity rate change pattern may be easy to find, a
820 collection of retrospective case studies - even a large collection - doesn't prove the
821 significance of an observed pattern. Statistical tests must be performed on a large dataset
822 and/or prospective testing must be undertaken. When testing the significance of observed
823 seismicity patterns, the null hypothesis must include comparisons with synthetic catalogs
824 with realistic spatiotemporal clustering.

825

826 Appendix: Catalogs with Synthetic Aftershocks

827 Producing synthetic catalogs with realistic spatiotemporal clustering is a complex task.
828 We based our simulations on the ETAS model [e.g. Ogata, 1988] which provides realistic
829 temporal clustering. To produce a realistic rate and spatial distribution of seismicity we
830 need to seed the ETAS clusters with background earthquakes and then spatially distribute
831 the events within the clusters.

832 The times of the background earthquakes are chosen randomly, using a spatially-
833 varying background seismicity rate found from the real ANSS catalog using the
834 technique of Hainzl *et al.* [2006]. The overall spatial character is less distinct in our

835 synthetic ETAS catalogs than for the real data because of the 0.5° grid used to compute
836 the spatially varying rate of background earthquakes (Figure 7a, g, and i). A smaller grid
837 size would produce more spatially focused seismicity patterns but at the expense of less
838 stable estimation of the background rates.

839 Since it has been found that 60% of the earthquake catalog is made up of easily
840 identifiable aftershocks [Gardner and Knopoff, 1974] the background seismicity rate
841 should be equal to about 40% of the total seismicity rate. The ANSS earthquake catalog
842 that we use has an average total seismicity rate of 67.2 $M \geq 4$ earthquakes per year from
843 1950-2005, leading to an estimated background rate of 26.9 $M \geq 4$ earthquakes/year. In
844 comparison, the Hainzl *et al.* [2006] method gives a total of 21.3 $M \geq 4$ background
845 earthquakes/year. The discrepancy may be because isolated areas with higher than
846 average aftershock/background ratios contribute heavily to the total, and because the
847 mainshock rate estimated by the Hainzl *et al.* [2006] method tends to be too low for
848 catalogs with certain aftershock parameters. We correct for the difference by multiplying
849 the background seismicity rates across the board by a factor of 1.26. Grid cells with no
850 seismicity were given a small rate of mainshocks such that in each simulation there is a
851 50% probability that one or more earthquakes will occur in the union of these grid cells.

852 The ETAS simulations are implemented using the inverse transform method of Felzer
853 *et al.* [2002]. In these simulations each earthquake, including each aftershock, may
854 produce its own aftershocks. The total number of aftershocks produced per mainshock
855 varies as $\sim 10^{bM}$, where M is mainshock magnitude and b is the b parameter in the
856 Gutenberg-Richter magnitude frequency relationship [Gutenberg and Richter, 1944]. In
857 the temporal domain the simulated aftershocks follow the modified Omori law [Utsu,

858 1961] given by $R(t) = K(t+c)^{-p}$, where t is time since the mainshock, R is the aftershock
859 rate, c and p are constants, and K is a value that varies with the magnitudes of the
860 mainshocks in question. Using the results of Felzer *et al.* [2002] we set $K=k10^{b(M-M_{aft})}$,
861 where M is mainshock magnitude, M_{aft} is the magnitude of the smallest aftershock
862 counted, and k is an activity constant that is independent of magnitude.

863 In Felzer *et al.* [2002] the smallest magnitude earthquake used in simulations, M_{min} ,
864 was set to M 0. Here we increase M_{min} to 2.5. This is because we are doing a large
865 simulation – over the entire states of California and Nevada for 55 years – and increasing
866 M_{min} by a few units of magnitude saves on computational time substantially while
867 preserving a realistic simulation. The change in M_{min} , however, also requires a
868 corresponding change in the direct modified Omori law parameters. Note that the direct
869 modified Omori parameters, which are the required input for the ETAS simulation, are
870 the parameters that describe the rate of triggering of direct aftershocks only; they do not
871 describe the combination of direct and secondary aftershocks that make up the full
872 aftershock sequences observed in the field. It is very difficult to tease apart individual
873 direct aftershock sequences from complete aftershock sequences observationally, making
874 most direct parameters difficult to measure. An exception is the direct p parameter. It
875 can be derived [Sornette and Sornette, 1999] and observed [Felzer *et al.*, 2003] that the p
876 parameter for complete aftershock sequences changes with time, such that the average p
877 value over a full sequence is close to 1.0 but the p value fit to data at long times is >1 and
878 tends to converge to the underlying direct p value. Felzer *et al.* [2003] found that
879 California p values converge to about 1.34 at long times. Thus we set our direct p value
880 to 1.34 and then grid search for the direct values of k and c . In the grid search the ETAS

881 simulation is run with incremented parameter values, and the results are checked against
882 the average ten and thirty day aftershock rates of $M \geq 4.7$ mainshocks in California. The
883 best fit parameters found for $M_{min}=2.5$ are $k=0.008 \text{ days}^{(1-p)}$ and $c = 0.095 \text{ days}$.

884 The ETAS simulations of Felzer *et al.* [2002] are performed completely in the
885 temporal domain. Here we add a spatial dimension by modeling each earthquake as a
886 fault plane in 3D, with rupture dimensions taken from the relationships of Wells and
887 Coppersmith [1994]. All faults are given a 90° dip, and 75% are randomly assigned a
888 303° strike (clockwise from north) and 25% a 213° strike, in accordance with our
889 estimate of major fault trends in California. Aftershocks are placed in space such that
890 their probability of being a distance, r , from the closest point on the fault plane of their
891 mainshock varies as $\sim r^{-1.3}$, in accordance with the empirical results of Felzer and
892 Brodsky, [2006]. Aftershock depth is limited to between 0 and 20 km. To avoid
893 singularity at $r = 0$ aftershocks are not allowed closer than 1 meter from the mainshock
894 fault plane.

895 For the magnitude distribution for the first set of simulations we follow Felzer *et al.*
896 [2002], and assign the magnitude of each earthquake randomly from the Gutenberg-
897 Richter distribution with a b value of 1.0. For the second set of simulations, we choose
898 magnitudes randomly from the magnitudes listed in the ANSS catalog. Note that the
899 total number of earthquakes in each ETAS simulation and in the ANSS catalog will not
900 necessarily be the same because there is Poissonian randomness and positive feedback in
901 the generation of ETAS aftershock sequences, leading to some unpredictability in total
902 catalog size. As a result, some magnitudes will be randomly omitted or repeated.

903 The ANSS catalog has some incompleteness at the smaller magnitudes and magnitude
904 error, both of which bias the magnitude distribution upwards [Tinti and Mulargia, 1985].
905 Thus when we use ANSS magnitudes in the ETAS simulations, the higher values cause
906 more aftershocks to be produced, and the simulated catalogs end up somewhat more
907 active than the real catalog. Whereas the real catalog contains 42 $M \geq 6$ mainshocks, for
908 example, the ETAS simulations with ANSS-source magnitudes have a mean of 52, and a
909 median of 49, $M \geq 6$ earthquakes per simulated catalog. When we perform the simulations
910 using magnitudes from the pure G-R distribution, on the other hand, neither input nor
911 output magnitudes are exaggerated and we end up with fewer than 42 mainshocks; a
912 median of 36 and a mean of 38 $M \geq 6$ earthquakes/simulated catalog. The standard
913 deviation, however, is quite large, with the smallest ANSS and G-R simulated catalogs
914 having only 19 and 25 $M \geq 6$ earthquakes, respectively, and the largest ones having 54 and
915 58. Thus our ETAS simulations span the number of earthquakes in the real catalog. To
916 insure that the variability in the total number of earthquakes per simulated catalog itself
917 will not affect our results we perform trials with purely random catalogs, altering the total
918 earthquake rate from 0.25 to 4 times that seen in the real ANSS catalog, and measuring
919 the value of C for random mainshocks in each trial. We find no correlation between C
920 values and the total number of earthquakes in the catalog over this range. In total for this
921 test, we perform 20 ETAS simulations with each of the magnitude assignment methods
922 described above. Hence, our ETAS simulations are sufficiently accurate for the purposes
923 of the tests done in this study.

924

925

925 Acknowledgments

926

927 We thank David Bowman and Arnaud Mignan for several productive discussions. We
928 are grateful to Sue Hough, Ken Hudnut, two anonymous reviewers, and the associate
929 editor for their helpful reviews of the manuscript. We thank Ross Stein for suggesting we
930 search for decelerating moment release. Several figures were prepared using the Generic
931 Mapping Tools [Wessel and Smith, 1998]. All authors contributed equally to this article
932 and the order was selected using a uniform random number generator.

933

934

934

935 References:

936

- 937 Allen, C. R., A. Grantz, J. N. Brune, M. M. Clark, R. V. Sharp, T. G. Theodore, E. W.
938 Wolfe, and M. Wyss (1968), The Borrego Mountain, California, earthquake of 9
939 April 1968: a preliminary report, *Bull. Seism. Soc. Am.*, 58, 1183-1186,
940 Benioff, H. (1951), Earthquakes and rock creep, part I, Creep characteristics of rocks and
941 the origin of aftershocks, *BSSA*, 41, 31-62,
942 Bowman, D. D., G. Ouillon, C. G. Sammis, A. Sornette, and D. Sornette (1998), An
943 observational test of the critical earthquake concept, *Journal of Geophysical*
944 *Research B: Solid Earth*, 103(10), 24359-24372,
945 Bowman, D. D., and G. C. P. King (2001), Accelerating seismicity and stress
946 accumulation before large earthquakes, *Geophys. Res. Lett.*, 28(21), 4039-4042,
947 Bufe, C. G., and D. J. Varnes (1993), Predictive modeling of the seismic cycle of the
948 greater San Francisco Bay region, *Journal of Geophysical Research*, 98, 9871-
949 9883,
950 Caskey, S. J., S. G. Wesnousky, P. Zhang, and D. B. Slemmons (1996), Surface faulting
951 of the 1954 Fairview Peak (Ms 7.2) and Dixie Valley (M (sub S) 6.8)
952 earthquakes, central Nevada, *Bull. Seism. Soc. Am.*, 86, 761-787,
953 Doser, D. I. (1986), Earthquake processes in the Rainbow Mountain-Fairview Peak-Dixie
954 Valley, Nevada, region 1954-1959, *Journal of Geophysical Research*, 91, 12,572-
955 512,586,
956 Ebel, J. E., and D. V. Helmberger (1982), P-wave complexity and fault asperities: the
957 Borrego Mountain, California, earthquake of 1968, *Bull. Seism. Soc. Am.*, 72,
958 413-437,
959 Felzer, K. R., T. W. Becker, R. E. Abercrombie, G. Ekstrom, and J. R. Rice (2002),
960 Triggering of the 1999 Mw 7.1 Hector Mine earthquake by aftershocks of the
961 1992 Mw 7.3 Landers earthquake, *Journal of Geophysical Research*, 107(B9),
962 10.1029/2001JB000911.
963 Felzer, K. R., R. E. Abercrombie, and G. Ekstrom (2003), Secondary aftershocks and
964 their importance for aftershock prediction, *Bull. Seism. Soc. Am.*, 93, 1433-1448,
965 Felzer, K. R., and E. E. Brodsky (2006), Decay of aftershock density with distance
966 indicates triggering by dynamic stress, *Nature*, 441, 735-738,
967 Gardner, J. K., and L. Knopoff (1974), Is the sequence of earthquakes in southern
968 California, with aftershocks removed, Poissonian?, *Bull. Seism. Soc. Am.*, 64,
969 1363-1367,
970 Gerstenberger, M., S. Wiemer, L. Jones, and P. Reasenberg (2005), Real-time forecasts
971 of tomorrow's earthquakes in California, *Nature*, 435, 328-331,
972 Gutenberg, B., and C. F. Richter (1944), Frequency of earthquakes in California, *Bull.*
973 *Seism. Soc. Am.*, 34(185-188),
974 Hainzl, S., F. Scherbaum, and C. Beauval (2006), Estimating background activity based
975 on interevent-time distribution, *Bull. Seism. Soc. Am.*, 96, 313-320,

- 976 Heaton, T., and D. V. Helmberger (1979), Generalized ray models of the San Fernando
977 earthquake, *Bull. Seism. Soc. Am.*, 69, 1311-1341,
- 978 Helmstetter, A., Y. Y. Kagan, and D. D. Jackson (2006), Comparison of short-term and
979 time-dependent earthquake forecast models for southern California, *Bull. Seism.
980 Soc. Am.*, 96, 90-106,
- 981 Ji, C., D. J. Wald, and D. V. Helmberger (2002), Source description of the 1999 Hector
982 Mine, California, earthquake, Part II: complexity of slip history, *Bull. Seism. Soc.
983 Am.*, 92, 1208-1226,
- 984 Ji, C., K. L. Larson, Y. Tan, K. W. Hudnut, and K. Choi (2004), Slip history of 2003 San
985 Simeon earthquake constrained by combining 1-Hz GPS, strong motion, and
986 teleseismic data, *Geophys. Res. Lett.*, 31, 10.1029/2004GL0120448.
- 987 Jiang, C., and Z. Wu (2005), Test of Preshock Accelerating Moment Release (AMR) in
988 the Case of the 26 December 2004 Mw9.0 Indonesia Earthquake, *Bull. Seism.
989 Soc. Am.*, 95, 2016-2025,
- 990 Kanamori, H., and D. L. Anderson (1975), Theoretical basis of some empirical relations
991 in seismology, *Bull. Seism. Soc. Am.*, 65, 1073-1095,
- 992 Kanamori, H. (1981), The nature of seismicity patterns before large earthquakes, in
993 *Earthquake Prediction An International Review*, edited by D. W. Simpson and P.
994 G. Richards, pp. 1-19, American Geophysical Union, Washington, D.C.
- 995 Keilis-Borok, V. I., and V. G. Kossobokov (1990), Times of increased probability of
996 strong earthquakes ($M \geq 7.5$) diagnosed by algorithm M8 in Japan and adjacent
997 territories, *JGR*, 95, 12,413-412,422,
- 998 King, G. C. P., and D. D. Bowman (2003), The evolution of regional seismicity between
999 large earthquakes, *Journal of Geophysical Research B: Solid Earth*, 108(2),
- 1000 Michael, A. J. (1997), Testing prediction methods; earthquake clustering versus the
1001 Poisson model, *Geophys. Res. Lett.*, 24(15), 1891-1894,
- 1002 Mignan, A., D. Bowman, and G. King (2006a), An observational test of the origin of
1003 accelerating moment release before large earthquakes, *Journal of Geophysical
1004 Research*, 111, B11304, doi:10.1029/2006JB004374.
- 1005 Mignan, A., G. King, D. Bowman, R. Lacassin, and R. Dmowska (2006b), Seismic
1006 activity in the Sumatra-Java region prior to the December 26, 2004 ($M_w = 9.0$ -
1007 9.3) and March 28, 2005 ($M_w = 8.7$) earthquakes, *Earth and Planetary Science
1008 Letters*, 244(3-4), 639-654,
- 1009 Ogata, Y. (1988), Statistical models of point occurrences and residual analysis for point
1010 processes, *J. Am. Stat. Assoc.*, 83, 9-27,
- 1011 Okada, Y. (1992), Internal deformation due to shear and tensile faults in a half-space,
1012 *Bull. Seism. Soc. Am.*, 82, 1018-1040,
- 1013 Reasenberg, P., and L. Jones (1994), Earthquake aftershocks: Update, *Science*, 265,
1014 1251-1252,
- 1015 Reasenberg, P. A., and M. V. Matthews (1988), Precursory seismic quiescence: a
1016 preliminary assessment of the hypothesis, *Pure & Applied Geophysics*, 126(2-4),
1017 373-406,
- 1018 Reasenberg, P. A., and L. M. Jones (1989), Earthquake hazard after a mainshock in
1019 California, *Science*, 243(4895), 1173-1176,

- 1020 Reyners, M. (1981), Long- and intermediate-term seismic precursors to earthquakes; state
1021 of the art, in Maurice Ewing Series, no.4, edited by D. W. Simpson and P. G.
1022 Richards, pp. 333-347.
- 1023 Savage, J. C., and R. O. Burford (1973), Geodetic Determination of Relative Plate
1024 Motion in Central California, *Journal of Geophysical Research*, 78, 832-845,
- 1025 Sornette, A., and D. Sornette (1999), Renormalization of earthquake aftershocks,
1026 *Geophys. Res. Lett.*, 26, 1981-1984,
- 1027 Tiampo, K. F., J. B. Rundle, W. Klein, and J. R. Holliday (2006), Forecasting rupture
1028 dimension using the pattern informatics technique, *Tectonophysics*, 424(3-4),
1029 367-376,
- 1030 Tinti, S., and F. Mulargia (1985), Effects of magnitude uncertainties on estimating
1031 parameters in the Gutenberg-Richter frequency-magnitude law, *Bull. Seism. Soc.*
1032 *Am.*, 75, 1681-1697,
- 1033 Topozada, T. R., and D. M. Branum (2002), California earthquakes of $M > 5$: their
1034 history and areas damaged, in *International Handbook of Earthquake and*
1035 *Engineering Seismology (Part A)*, edited by W. H. K. Lee, et al., pp. 793-796.
- 1036 Uhrhammer, R. A., S. J. Lober, and B. Romanowicz (1996), Determination of local
1037 magnitude using BDSN broadband records, *Bull. Seism. Soc. Am.*, 86, 1314-
1038 1330,
- 1039 Utsu, T. (1961), A statistical study on the occurrence of aftershocks, *Geophysical*
1040 *Magazine*, 30, 521-605,
- 1041 Wald, D. J., D. V. Helmberger, and S. Hartzel (1990), Rupture process of the 1987
1042 Superstition Hills earthquake from the inversion of strong-motion data, *Bull.*
1043 *Seism. Soc. Am.*, 81, 1540-1572,
- 1044 Wald, D. J., D. V. Helmberger, T. H. Heaton, T. C. Hanks, and H. Krawinkler (1991),
1045 Rupture model of the 1989 Loma Prieta earthquake from the inversion of strong-
1046 motion and broadband teleseismic data, *Bull. Seism. Soc. Am.*, 81(5), 1540-1572,
- 1047 Wald, D. J., and T. Heaton (1994), Spatial and temporal distribution of slip for the 1992
1048 Landers, California, earthquake, *Bull. Seism. Soc. Am.*, 84, 668-691,
- 1049 Wald, D. J., T. Heaton, and K. W. Hudnut (1996), The slip history of the 1994
1050 Northridge, California, earthquake determined from strong-motion, teleseismic,
1051 GPS, and leveling data, *Bull. Seism. Soc. Am.*, 86, S49-S70,
- 1052 Wells, D. L., and K. J. Coppersmith (1994), New empirical relationships among
1053 magnitude, rupture length, rupture width, rupture area, and surface displacement,
1054 *Seismological Society of America Bulletin*, 84(4), 974-1002,
- 1055 Wessel, P., and W. H. F. Smith (1998), New, improved version of the Generic Mapping
1056 Tools released, *EOS*, 79, 579,
1057
1058

1058
1059 Figures:

1060

1061 Figure 1. Example of fitting a power-law (red, dashed line) and linear function (black
1062 line) to the data (blue circles). For this example, which is from an ETAS simulation
1063 of an earthquake catalog, $C = 0.4$.

1064 Figure 2. Map showing the region analyzed with earthquakes $M \geq 4$ as black dots,
1065 earthquakes $M \geq 6$ as red stars, mainshocks analyzed in Bowman *et al.* [1998] as blue
1066 stars, mainshocks included in our test of searching for AMR based on prestress
1067 patterns as blue circles, and faults and state borders as lines.

1068 Figure 3. C versus radius, for the 1992 Landers earthquake, with both 10 and 20 km
1069 search steps, using all events $M \geq 4$. The beginning of the time interval is fixed to
1070 1970, which produces the lowest C -value over all start times and radii. The total
1071 number of events, N , is also shown.

1072 Figure 4. Optimal decelerating moment release (DMR) curves for the 8 California $M \geq 6.5$
1073 mainshocks for which Bowman et al [1998] report AMR. C is the curvature
1074 parameter, and R is the optimal radius.

1075 Figure 5. Cumulative distribution of the observed curvature parameter C for the optimal
1076 AMR (black lines) and DMR (red dashed lines) before each $M \geq 6$ mainshock in the
1077 ANSS catalog for California and Nevada, since 1950. The thick lines show the best
1078 result and the thin lines show the 95% confidence region determined by bootstrap
1079 resampling.

1080 Figure 6. Optimal AMR and DMR for the December 2004 M9.1 Sumatra earthquake,
 1081 using minimum magnitudes of 4.5 and 5.5. C is the curvature parameter, and R is the
 1082 optimal radius. Note that the data is not complete to magnitude 4.5; but that level is
 1083 included for comparison to Mignan *et al.* [2006b].

1084 Figure 7. Maps and time series of the real data from the ANSS catalog and examples of
 1085 the four simulation methods used in the paper. The maps show earthquakes $M \geq 4$ as
 1086 black dots, earthquakes $M \geq 6$ as red stars, and faults and state borders as lines. The
 1087 time series show the number of earthquakes per month with the occurrence of
 1088 earthquakes $M \geq 6$ as red stars.

1089 Figure 8. Cumulative distribution of the observed curvature parameter C for the optimal
 1090 AMR determined from the real ANSS catalog (black lines) and each of the four
 1091 simulation methods (red dashed lines) before each $M \geq 6$ mainshock. Results for both
 1092 $N_{min} = 4$ and $N_{min} = 10$ are shown. The thick lines show the best result and the thin
 1093 lines show the 95% confidence region determined by bootstrap resampling. The
 1094 confidence is the level at which we can reject the null hypothesis that the C -values for
 1095 the real data are not lower than the C -values for the synthetic data, e.g. the confidence
 1096 of accepting AMR.

1097 Figure 9. Parameters for optimal AMR for the real California-Nevada catalog, for $N_{min}=4$
 1098 (red) and $N_{min}=10$ (black). (a) Number of events in the optimal sequence, N , versus
 1099 C . Lines connect points for the same mainshock for different N_{min} . (b) Cumulative
 1100 distribution of the power-law exponent m . (c) N versus m . (d) C versus m .

1101 Figure 10. Optimal AMR radius and duration versus mainshock magnitude, for eight
 1102 $M \geq 6.5$ California earthquakes. Scaling relations were found by least-squares fit of

1103 log-radius or log-duration versus magnitude. Correlation coefficient (r) and
 1104 significance of correlation also shown. (a) Optimal radii from Bowman et al. [1998],
 1105 found using catalogs with minimum magnitude 2 units below mainshock magnitude.
 1106 Solid line, fit to the 8 California earthquakes; dashed line, Bowman et al.'s [1998] fit
 1107 including 4 additional mainshocks to extend the magnitude range. (b) Optimal AMR
 1108 durations from Bowman et al. [1998]. (c) and (d) The optimal radius and duration
 1109 for each mainshock, found using catalogs with fixed minimum magnitude of $M_{4.0}$.
 1110 Optimization was performed by grid search to minimize the misfit parameter C .

1111 Figure 11. Cumulative distribution of the observed curvature parameter C for optimal
 1112 AMR, fixing $m=0.3$. Distributions are shown for the real ANSS catalog (black lines)
 1113 and the ETAS simulation methods with G-R magnitudes (red dashed lines) before
 1114 each $M \geq 6$ mainshock. Results for both $N_{min} = 4$ and $N_{min} = 10$ are shown. The thick
 1115 lines show the best result and the thin lines show the 95% confidence region
 1116 determined by bootstrap resampling. The confidence is the level at which we can
 1117 reject the null hypothesis that the C -values for the real data are not lower than the C -
 1118 values for the synthetic data, e.g. the confidence of accepting AMR.

1119 Figure 12. (a) Cumulative number of earthquakes with $M \geq 4.0$ in the ANSS catalog and a
 1120 ETAS simulation using a Gutenberg-Richter distribution for the magnitudes. Solid
 1121 lines show the complete catalogs while the dashed lines show the result of
 1122 declustering. (b) Cumulative distribution of the observed curvature parameter C for
 1123 the optimal AMR determined from the real declustered ANSS catalog (black lines)
 1124 and the declustered ETAS simulations (red dashed lines) before each $M \geq 6$
 1125 mainshock. Results for $N_{min} = 10$ are shown. The thick lines show the best result and

1126 the thin lines show the 95% confidence region determined by bootstrap resampling.
1127 The confidence is the level at which we can reject the null hypothesis that the C -
1128 values for the real data are not lower than the C -values for the synthetic data, e.g. the
1129 confidence of accepting AMR.
1130

1130 Tables:

1131 Table 1. Optimal length-scale and time-scale for AMR [from Bowman *et al.*, 1998] and

1132 DMR (this study) for 8 California mainshocks.

1133

| Earthquake mon/day/yr | AMR length- scale (km) [Bowmann et al, 1998] | AMR length- scale (km) [this study] | DMR length- scale (km) | AMR time-scale (yr) [Bowman et al, 1998] | AMR time- scale (yr) [this study] | DMR time- scale (yr) |
|---------------------------|---|--|---------------------------------|---|---|----------------------------|
| Kern County 7/21/1952 | 325 | 360 | 720 | 42 | 42 | 14 |
| Landers 6/28/1992 | 150 | 40 | 120 | 22 | 44 | 49 |
| Loma Prieta 10/18/1989 | 200 | 60 | 300 | 79 | 79 | 7 |
| Coalinga 5/2/1983 | 175 | 180 | 140 | 3 | 4 | 12 |
| Northridge 1/17/1994 | 73 | 380 | 120 | 2 | 38 | 6 |
| San Fernando 2/9/1971 | 100 | 140 | 420 | 4 | 9 | 21 |
| Superstition | 275 | 100 | 160 | 6 | 7 | 9 |

| | | | | | | |
|--------------------------|-----|-----|-----|----|---|----|
| Hills 11/24/1987 | | | | | | |
| Borrego Mtn. 4/9/1968 | 240 | 280 | 800 | 10 | 9 | 15 |

1134

1135 Table 2. Minimum value of C for earthquakes in the positive prestress regions, compared
 1136 to minimum C for all events. Lowest C value for each mainshock in bold.

1137

| Mainshock (mon/day/yr) | C , Positive Prestress Events | C , All Events |
|--------------------------------|---------------------------------|------------------|
| Fairview Peak, 12/16/1954 | 0.28 | 0.43 |
| Loma Prieta, 10/18/1989 | 0.35 | 0.43 |
| Hector Mine, 10/16/1999 | 0.61 | 0.68 |
| San Fernando, 2/9/1971 | 0.52 | 0.52 |
| San Simeon, 12/22/2003 | 0.7 | 0.6 |
| Borrego Mtn, 4/9/1968 | 1.0 | 0.53 |
| Landers, 6/28/1992 | 0.42 | 0.32 |
| Northridge, 1/17/1994 | 0.85 | 0.27 |
| Superstition Hills, 11/24/1987 | 0.24 | 0.05 |

1138

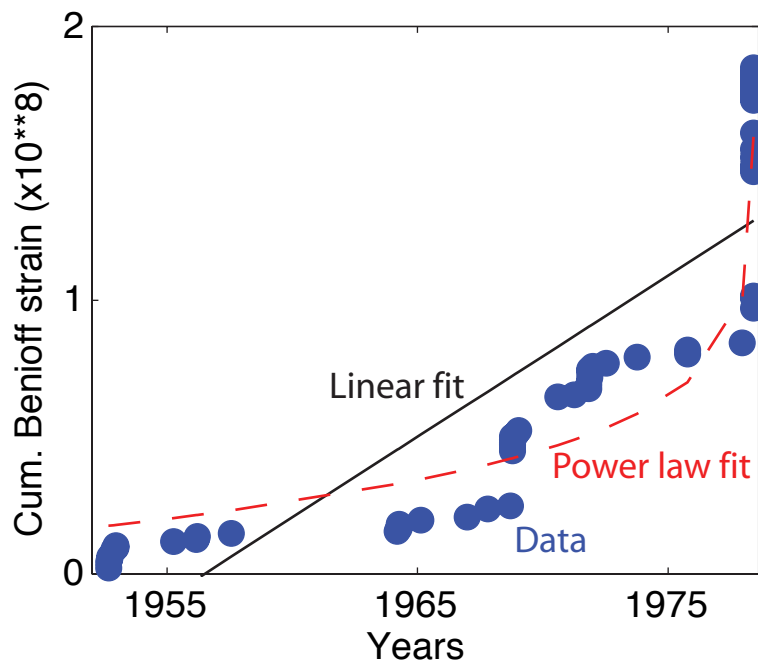


Figure 1. Example of fitting a power-law (red, dashed line) and linear function (black line) to the data (blue circles). For this example, which is from an ETAS simulation of an earthquake catalog, $C = 0.4$.

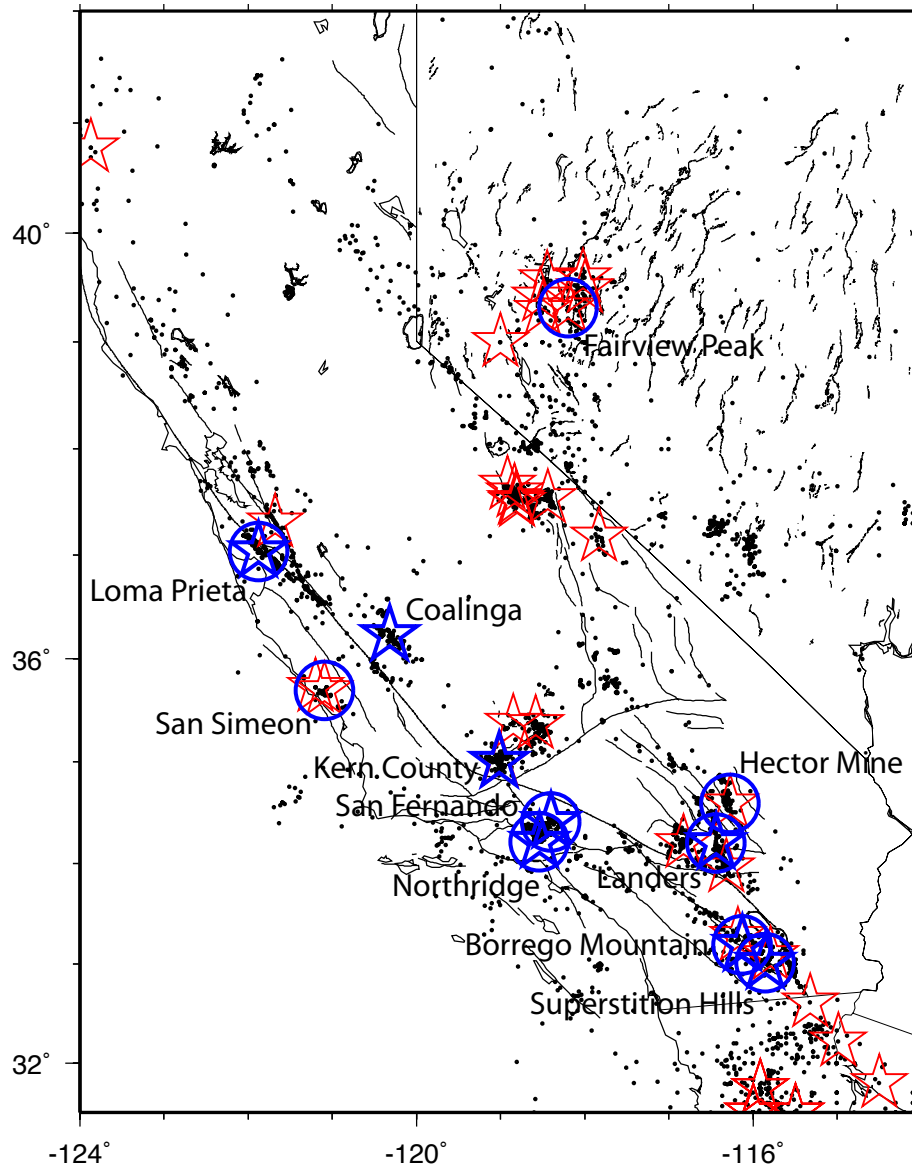


Figure 2. Map showing the region analyzed with earthquakes $M \geq 4$ as black dots, earthquakes $M \geq 6$ as red stars, mainshocks analyzed in Bowman *et al.* [1998] as blue stars, mainshocks included in our test of searching for AMR based on prestress patterns as blue circles, and faults and state borders as lines.

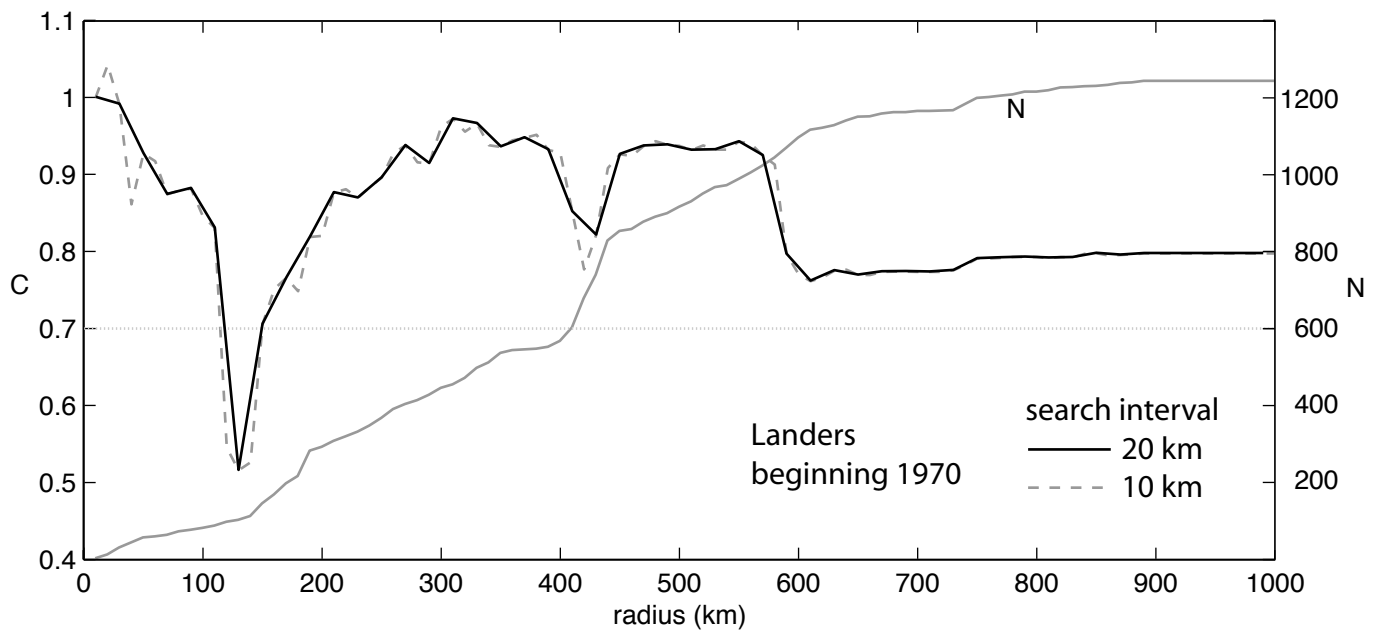


Figure 3. C versus radius, for the 1992 Landers earthquake, with both 10 and 20 km search steps, using all events $M \geq 4$. The beginning of the time interval is fixed to 1970, which produces the lowest C -value over all start times and radii. The total number of events is also shown.

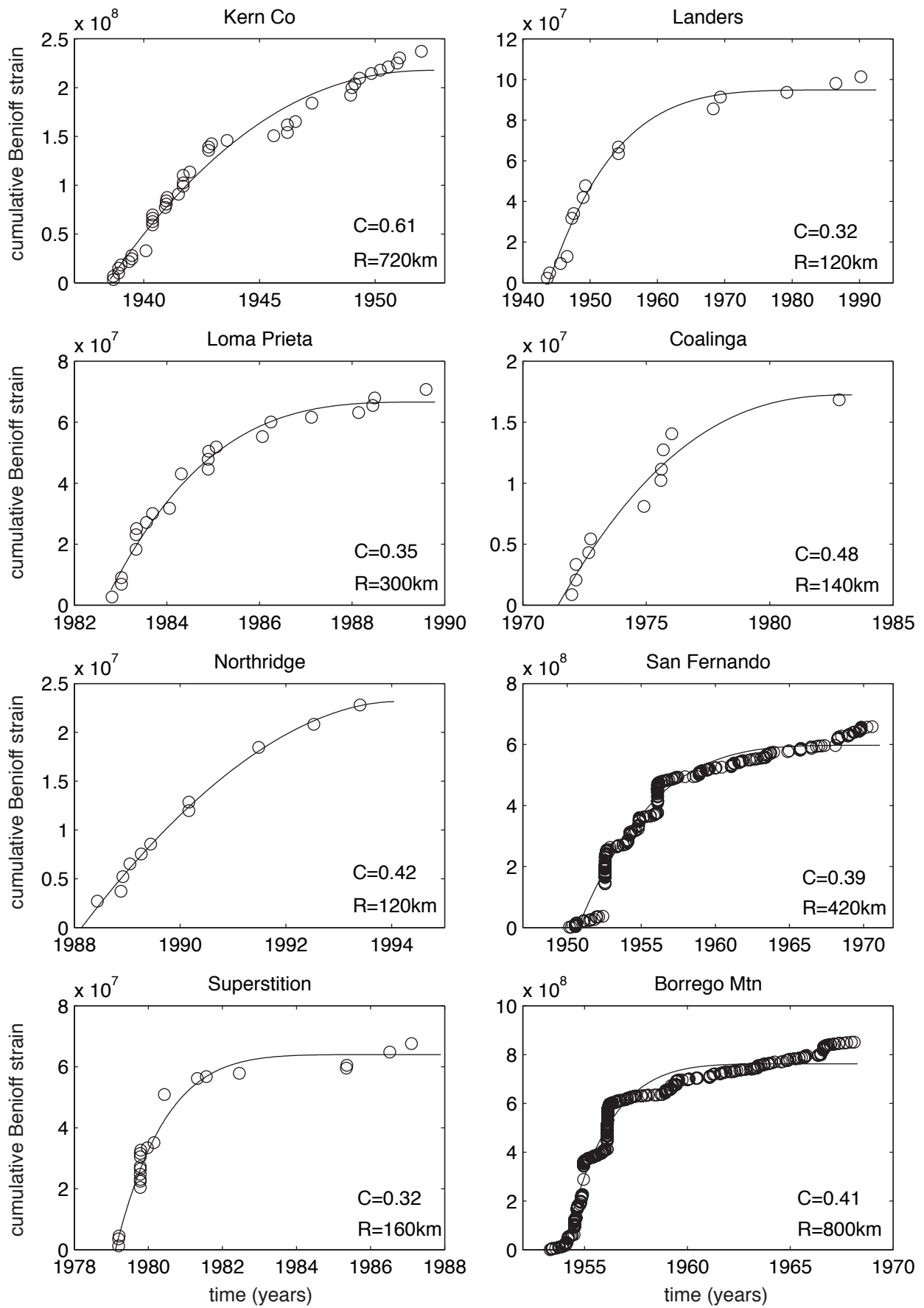


Figure 4. Optimal decelerating moment release (DMR) curves for the 8 California $M \geq 6.5$ mainshocks for which Bowman *et al.* [1998] report AMR. C is the curvature parameter, and R is the optimal radius.

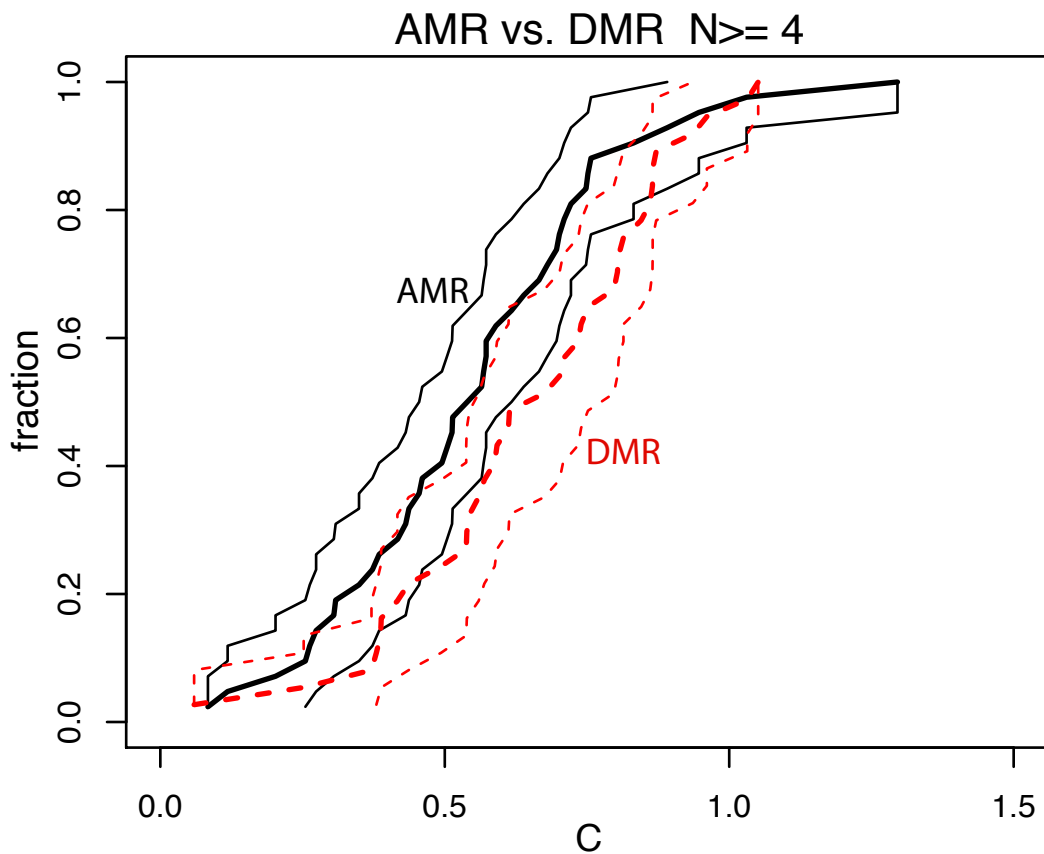


Figure 5. Cumulative distribution of the observed curvature parameter C for the optimal AMR (black lines) and DMR (red dashed lines) before each $M \geq 6$ mainshock in the ANSS catalog for California and Nevada, since 1950. The thick lines show the best result and the thin lines show the 95% confidence region determined by bootstrap resampling.

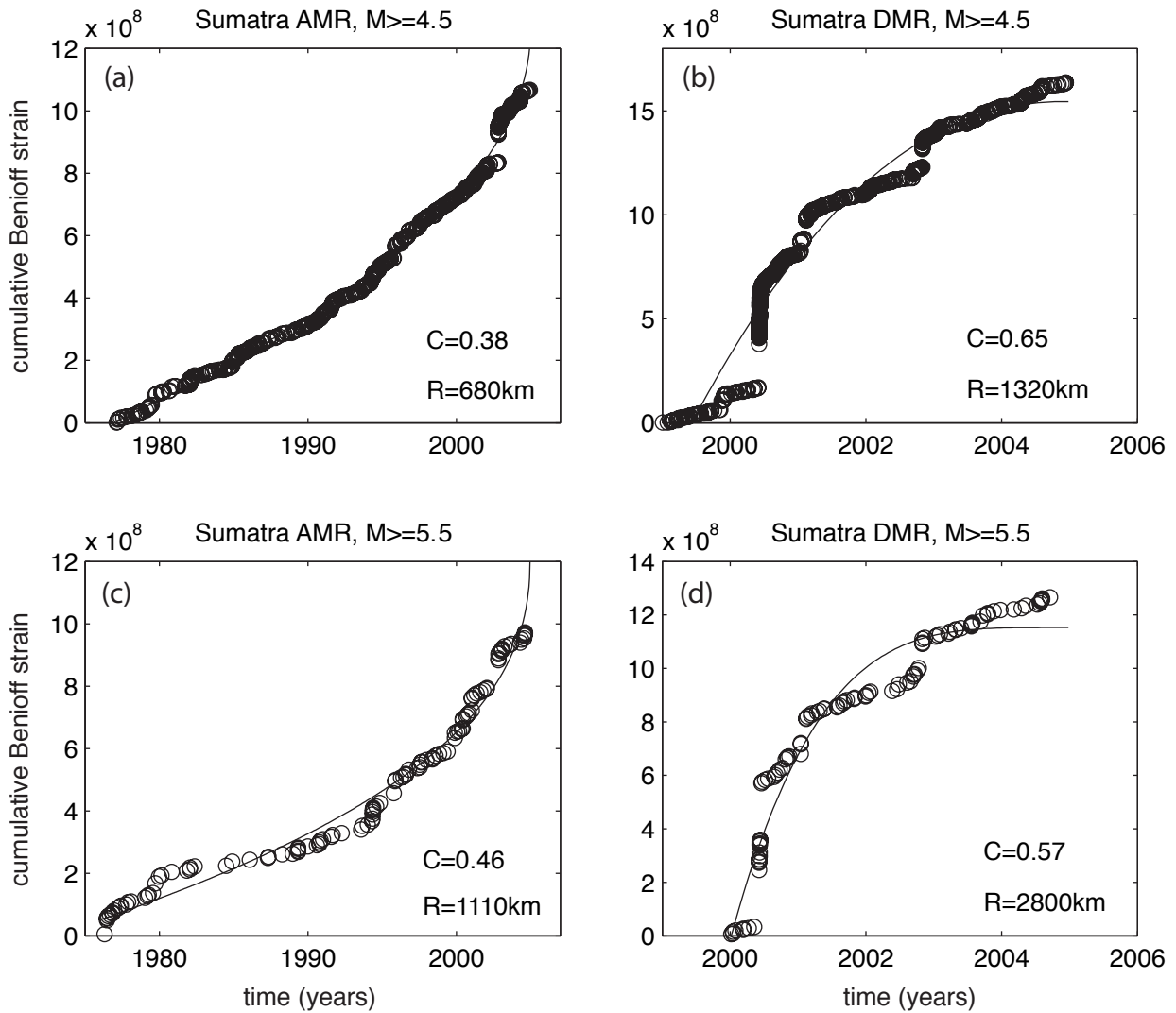


Figure 6. Optimal AMR and DMR for the December 2004 M9.1 Sumatra earthquake, using minimum magnitudes of 4.5 and 5.5. C is the curvature parameter, and R is the optimal radius. Note that the data is not complete to magnitude 4.5; but that level is included for comparison to Mignan *et al.* [2006b].

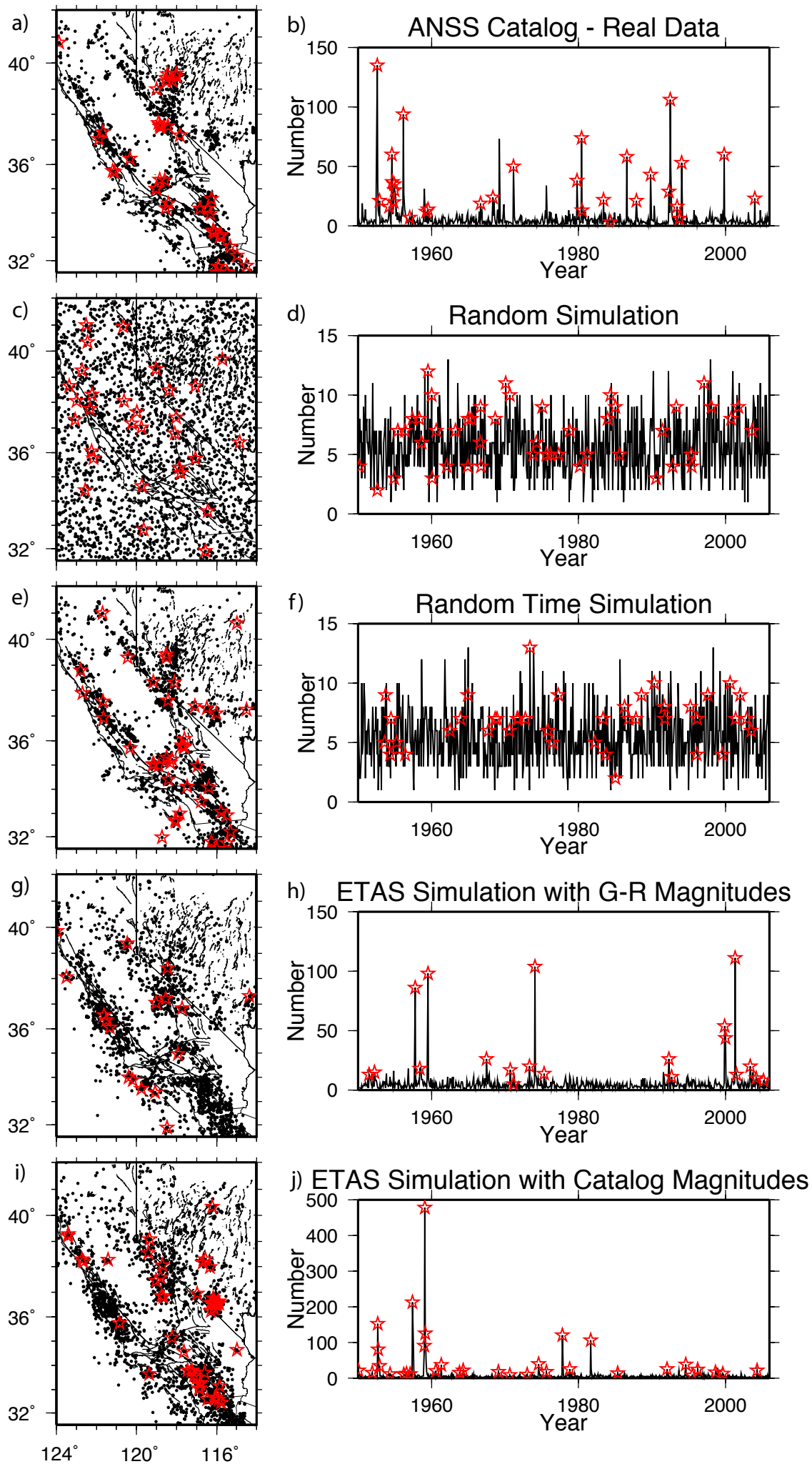


Figure 7. Maps and time series of the real data from the ANSS catalog and examples of the four simulation methods used in the paper. The maps show earthquakes $M \geq 4$ as black dots, earthquakes $M \geq 6$ as red stars, and faults and state borders as lines. The time series show the number of earthquakes per month with the occurrence of earthquakes $M \geq 6$ as red stars.

Figure 7

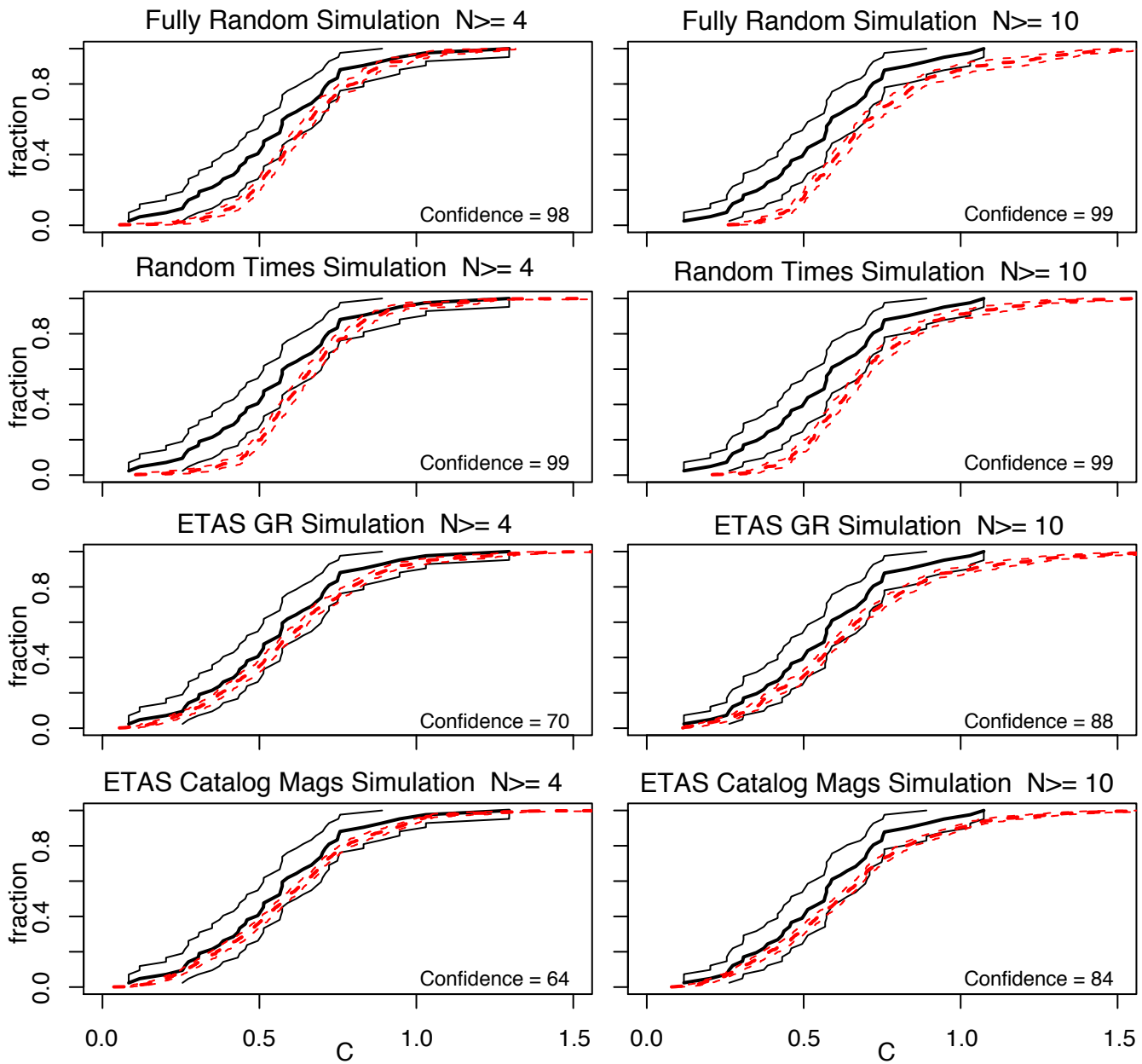


Figure 8. Cumulative distribution of the observed curvature parameter C for the optimal AMR determined from the real ANSS catalog (black lines) and each of the four simulation methods (red dashed lines) before each $M \geq 6$ mainshock. Results for both $N_{\min} = 4$ and $N_{\min} = 10$ are shown. The thick lines show the best result and the thin lines show the 95% confidence region determined by bootstrap resampling. The confidence is the level at which we can reject the null hypothesis that the C -values for the real data are not lower than the C -values for the synthetic data, e.g. the confidence of accepting AMR.

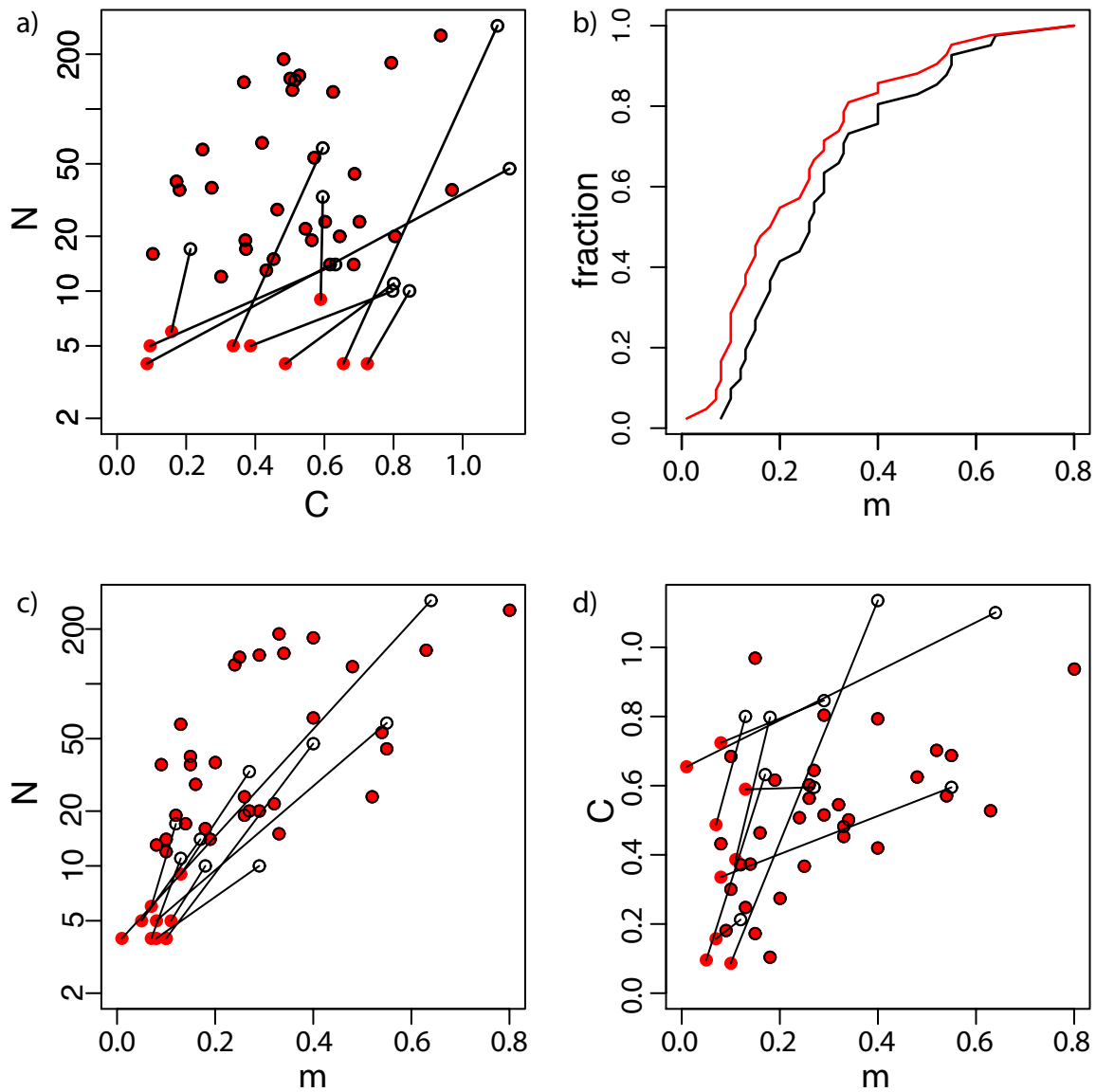


Figure 9. Parameters for optimal AMR for the real California-Nevada catalog, for $N_{min}=4$ (red) and $N_{min}=10$ (black). (a) Number of events in the optimal sequence, N , versus C . Lines connect points for the same mainshock for different N_{min} . (b) Cumulative distribution of the power-law exponent m . (c) N versus m . (d) C versus m .

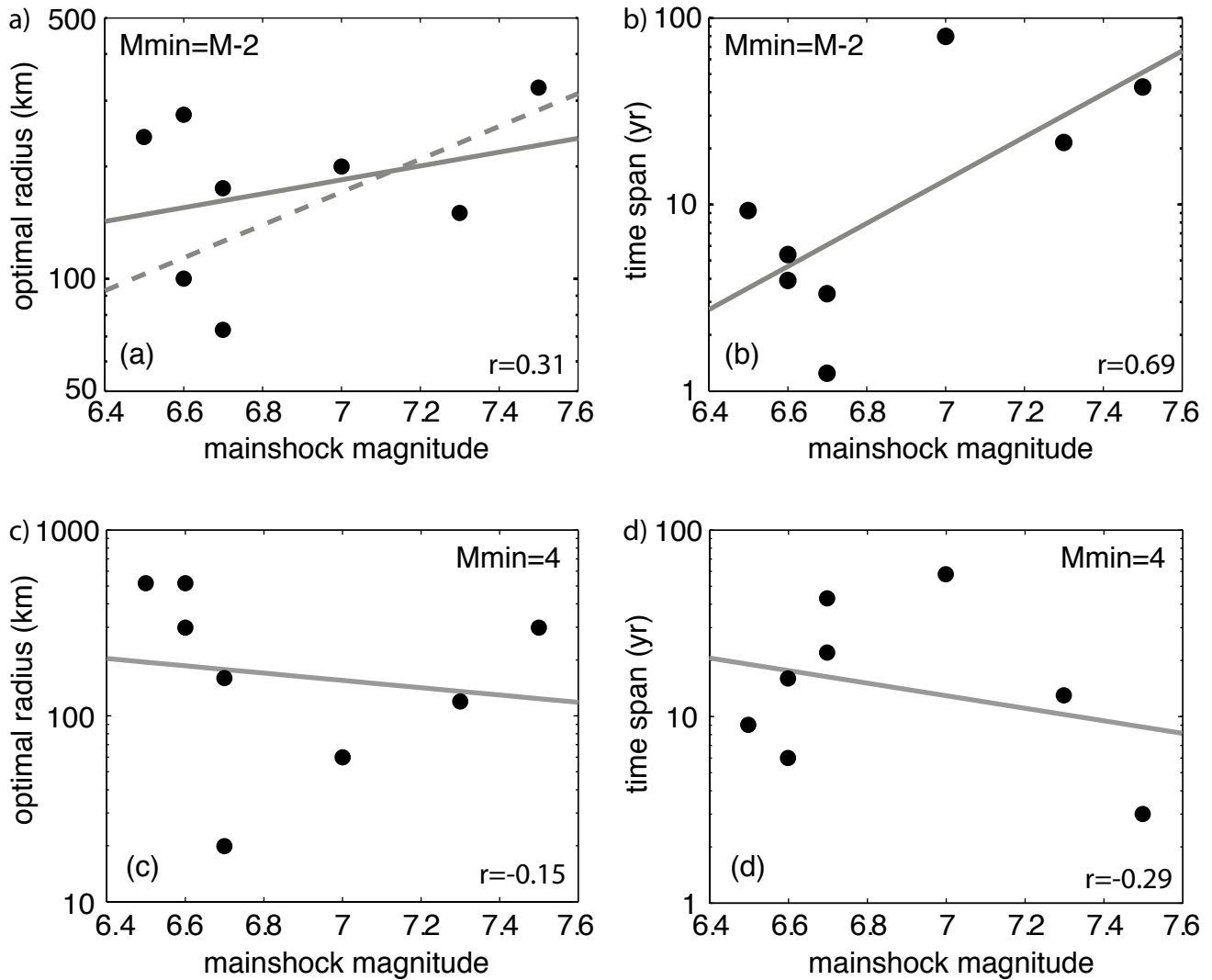


Figure 10. Optimal AMR radius and duration versus mainshock magnitude, for eight $M \geq 6.5$ California earthquakes. Scaling relations were found by least-squares fit of log-radius or log-duration versus magnitude. Correlation coefficient (r) and significance of correlation also shown. (a) Optimal radii from Bowman *et al.* [1998], found using catalogs with minimum magnitude 2 units below mainshock magnitude. Solid line, fit to the 8 California earthquakes; dashed line, Bowman *et al.*'s [1998] fit including 4 additional mainshocks to extend the magnitude range. (b) Optimal AMR durations from Bowman *et al.* [1998]. (c) and (d) The optimal radius and duration for each mainshock, found using catalogs with fixed minimum magnitude of $M4.0$. Optimization was performed by grid search to minimize the misfit parameter C .

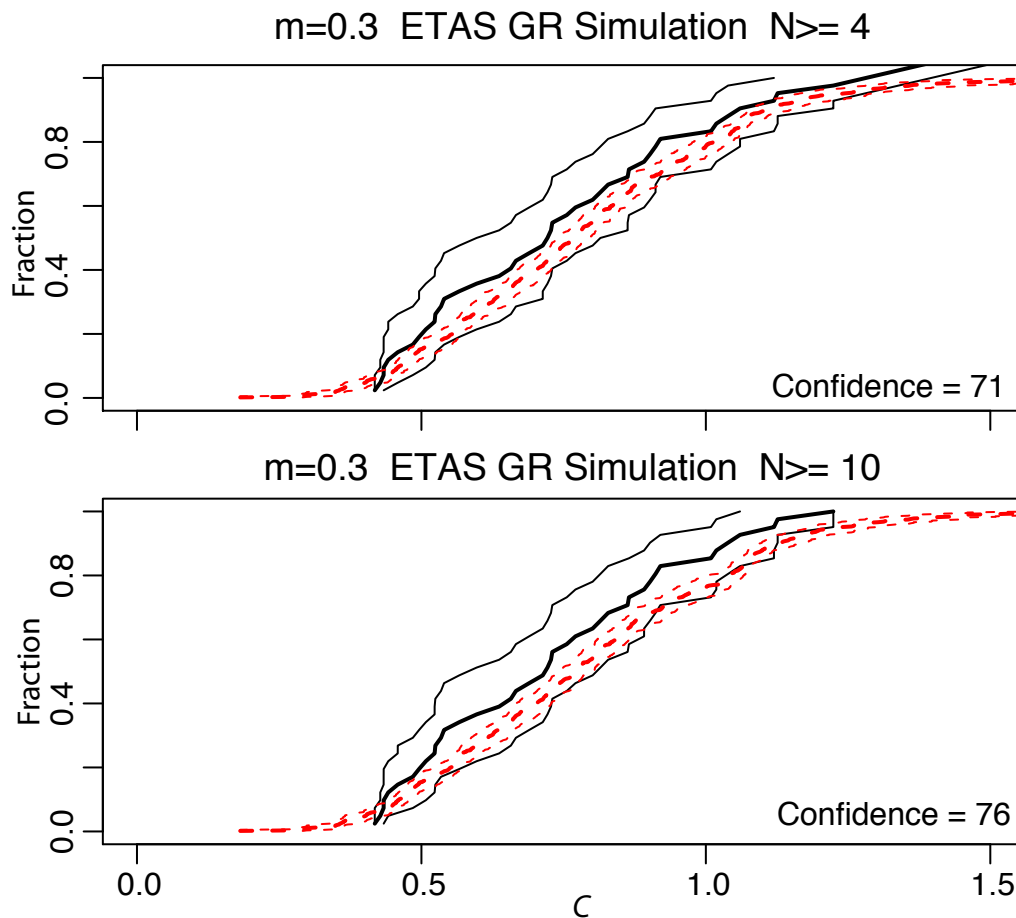


Figure 11. Cumulative distribution of the observed curvature parameter C for optimal AMR, fixing $m=0.3$. Distributions are shown for the real ANSS catalog (black lines) and the ETAS simulation methods with G-R magnitudes (red dashed lines) before each $M \geq 6$ mainshock. Results for both $N_{\min} = 4$ and $N_{\min} = 10$ are shown. The thick lines show the best result and the thin lines show the 95% confidence region determined by bootstrap resampling. The confidence is the level at which we can reject the null hypothesis that the C -values for the real data are not lower than the C -values for the synthetic data, e.g. the confidence of accepting AMR.

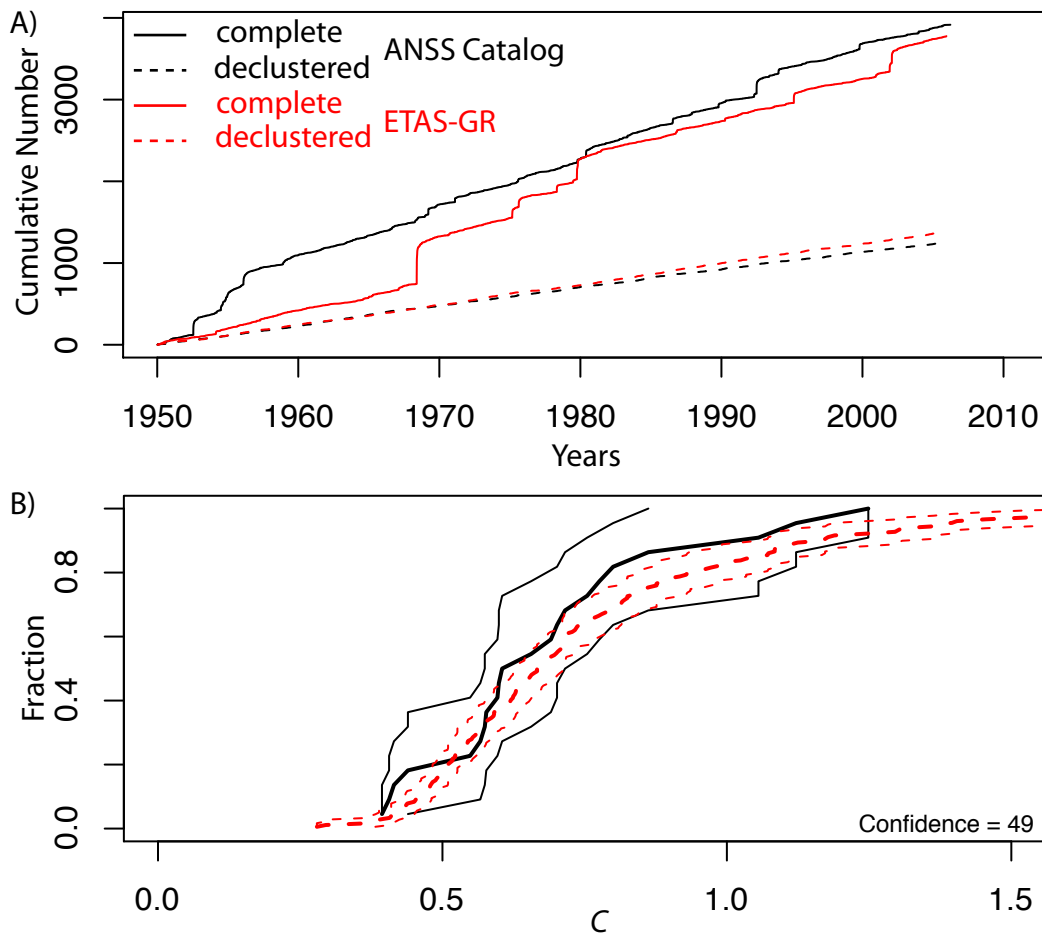


Figure 12. (a) Cumulative number of earthquakes with $M \geq 4.0$ in the ANSS catalog and a ETAS simulation using a Gutenberg-Richter distribution for the magnitudes. Solid lines show the complete catalogs while the dashed lines show the result of declustering. (b) Cumulative distribution of the observed curvature parameter C for the optimal AMR determined from the real declustered ANSS catalog (black lines) and the declustered ETAS simulations (red dashed lines) before each $M \geq 6$ mainshock. Results for $N_{\min} = 10$ are shown. The thick lines show the best result and the thin lines show the 95% confidence region determined by bootstrap resampling. The confidence is the level at which we can reject the null hypothesis that the C -values for the real data are not lower than the C -values for the synthetic data, e.g. the confidence of accepting AMR.